Title
71 ' PRODUCTION IN n+ d INTERACTIONS FROM THRESHOLD TO 2.4 GeV/c.

Author
Rader, Robert K.

Publication Date
1969-12-01

UCRL-19431

c.2

η' PRODUCTION IN $\pi^+ d$ INTERACTIONS FROM THRESHOLD TO 2.4 GeV/c

Robert K. Rader
(Ph.D. Thesis)

December 1969

AEC Contract No. W-7405-eng-48

LAWRENCE RADIATION LABORATORY
UNIVERSITY of CALIFORNIA BERKELEY

UCRL-19431

DISCLAIMER

η' PRODUCTION IN $\pi^+ d$ INTERACTIONS FROM THRESHOLD TO 2.4 GeV/c

Contents

η' Production in $\pi^+ d$ Interactions from Threshold to 2.4 GeV/c

Robert K. Rader

Lawrence Radiation Laboratory

University of California

Berkeley, California

ABSTRACT

We have studied η' production as part of an experiment using a π^+ beam incident on deuterium in the 72-in. bubble chamber, with beam momenta from 1.1 to 2.4 GeV/c. The η' is produced in the reaction $\pi^+ d \rightarrow pp\eta'$, and we observe the decay mode $\eta' \rightarrow \pi^+\pi^-\eta$. The reaction $\pi^+ n \rightarrow p\eta'$ is studied by using the spectator model. The cross section for $\pi^+ n \rightarrow p\eta'$ is observed to rise to a maximum of about 100 μb at 2.2 GeV c.m. energy. The production angular distribution develops peripheral peaking with increasing energy.

I. INTRODUCTION

We have studied η' production in $\pi^+ d$ interactions as a part of a 250 000 picture bubble chamber experiment, performed in the 72-in. deuterium filled bubble chamber, at the Lawrence Radiation Laboratory, Berkeley. A separated π^+ beam from the Bevatron was used, at beam momenta from 1.1 to 2.4 GeV/c, in approximately 0.2 GeV/c steps. In this paper the 5- and 6-prong events are used to study the reaction $\pi^+ d \to pp\eta'$, $\eta' \to \pi^+\pi^-\eta$, $\eta \to \pi^+\pi^-\pi^o$ or $\pi^+\pi^-\gamma$. The data available from the 3- and 4-prong events on this reaction, where the η decays into only neutral particles, is also presented.

This experiment was designed to study the production of the known $I = 0$, nonstrange mesons η, ω, and η', in $\pi^+ n$ interactions from 1.7 to 2.4 GeV center of mass (c.m.) energy. These processes cannot be analyzed in the charge-symmetric $\pi^- p$ interactions because then there are two neutral particles in the final state. The observed η and ω production is reported in ref. 1. Strange particle production has been studied and is reported in ref. 2. For further references to work published from this experiment, and other $\pi^+ d$ studies, see the compilation in ref. 1.

Interest in η' production in $\pi^+ n$ interactions was generated in early 1966, when it was observed that the reaction $\eta' \to \pi^+\pi^-\gamma$ is a good place to look for a violation of charge-conjugation invariance in electromagnetic decays. To plan an experiment using the reaction $\pi^- p \to n\eta'$, one needs to know the cross section for

this process. This reaction cannot be analyzed in a bubble chamber, and the cross section was not known. Since the charge-symmetric reaction $\pi^+ n \rightarrow p\eta'$ can be observed and analyzed in $\pi^+ d$ interactions in a bubble chamber, the present experiment was designed with the observation of this reaction as one of its goals.

The gathering and reduction of the data in this experiment are described in Section II. The final states and separation of hypotheses in the 5- and 6- prong events are discussed in Section III. The determination of final state cross sections is discussed in Section IV, and η' production is discussed in Section V. The results are summarized in Section VI.

II. EXPERIMENTAL PROCEDURES

A. The Beam

The separated π^+ beam used in this experiment was designed by W. Chinowsky, G. Smith, and J. Kirz (see the Bevatron Experimenter's Handbook, Section C, Bevatron Secondary Beam 1B, December, 1965). The major modification of the beam for our experiment was the use of a "stepper" magnet. Bubble chamber pictures are more easily scanned and measured if the beam tracks are separated by a few centimeters in space. To accomplish this, a narrow "pencil" beam was produced, and then stepped across the chamber by increasing the current in a specially-built magnet each time a beam particle was counted entering the chamber. The stepper magnet was used in the experimental runs from 1.3 to 2.4 GeV/c.

B. Beam Momenta and Pathlengths

The experiment was run in eight beam momentum settings, nominally from 1.1 to 2.3 GeV/c in steps of 0.2 GeV/c. Due to the Fermi motion of the nucleons in the deuteron, and the 40 MeV/c momentum loss in passing through the chamber, this would give a complete coverage of c.m. energies for the reactions on a nucleon, from 1.7 to 2.4 GeV.

The actual beam momenta were measured approximately as we ran the experiment, from small samples of film and a rough fitting program, and were later determined accurately for use in beam averaging in the fitting program. The median values of the beam

Table 1. Beam momenta and pathlengths.

Beam Momentum (GeV/c)	Pathlength (events/μb)	Error in Pathlength (events/μb)
1.10	0.45	0.03
1.30	0.44	0.03
1.53	2.53	0.13
1.58	0.43	0.04
1.70	3.03	0.16
1.86	2.92	0.15
2.15	3.09	0.13
2.37	0.84	0.08

momenta at the center of the chamber were determined by using a large sample of four-constraint fitted events from the 4-prong events measured on the Spiral Reader. The beam momenta are given in Table 1.

We used a special cross section scan to determine the total number of interactions, by topology, on a sample of film. The actual length of track was also measured. From these data the pathlength has been determined in several ways. The final values are given in Table 1, by momentum. These values agree with the several pathlength determinations.[3,4]

C. Scanning and Measuring

The film was scanned for non-strange events (3-, 4-, 5-, and 6-prong events), and events with one or two visible neutral particle decays (vees).[5] The scanned events were measured either on a Franckenstein measuring projector, or on the Spiral Reader.[6] The 5- and 6-prong events were all measured on the Franckenstein measuring projector, and the 3- and 4-prong events were all measured on the Spiral Reader. Figure 1 shows an example of a 6-prong event. The number of valid 5- and 6-prong events found in the scan is given by beam momentum in Table 2.

D. Geometric Reconstruction and Kinematic Fitting

Three pictures are taken of the bubble chamber from different angles each time the chamber is expanded, to make possible the geometric reconstruction of events. The geometric reconstruction

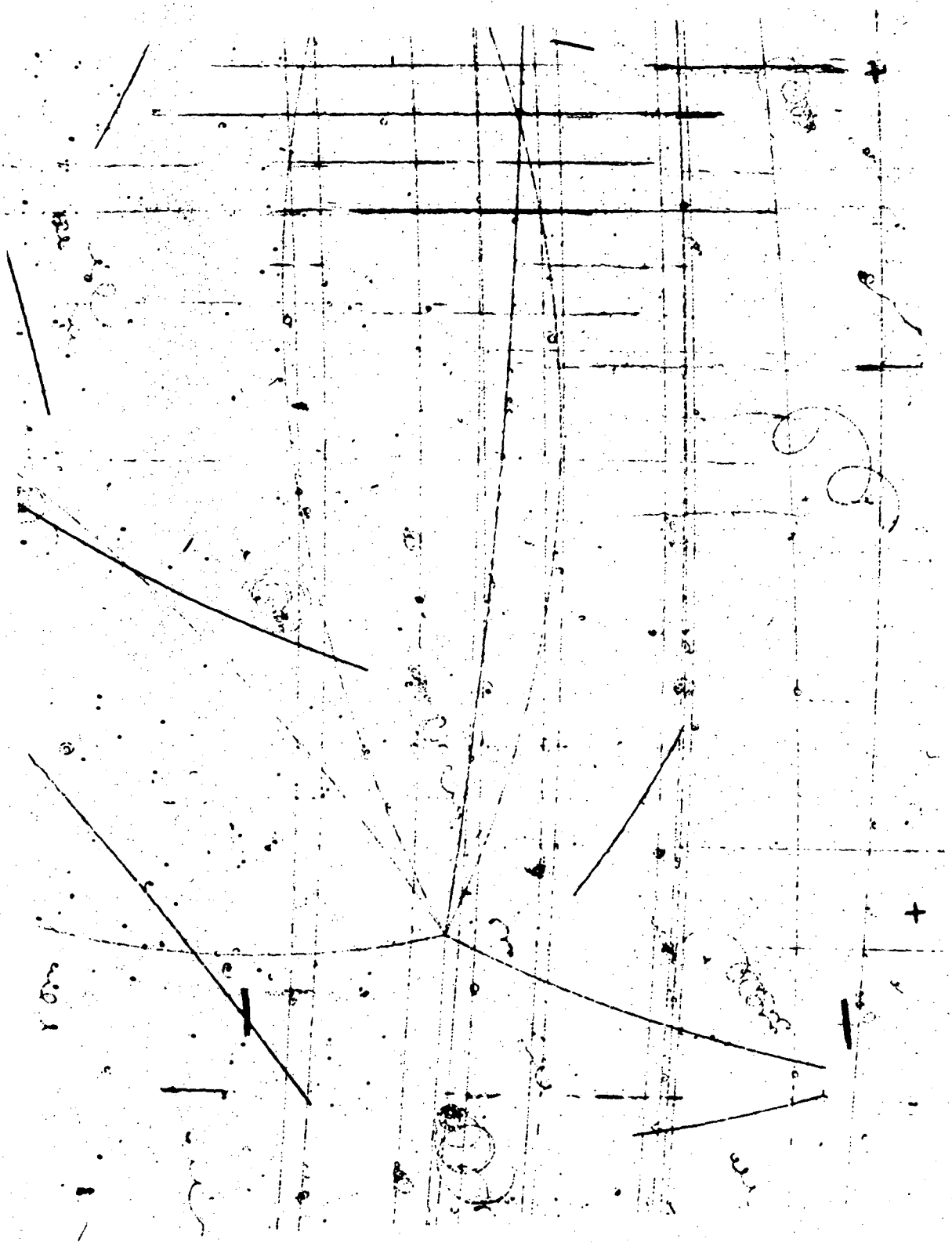

Figure 1. An example of a 6-prong event.

Table 2. Number of 5- and 6-prong events found in scan.

Beam Momentum (GeV/c)	Number of events
1.10	3
1.30	11
1.53	171
1.58	46
1.70	478
1.86	751
2.15	1638
2.37	636

of the particle tracks is done by TVGP[7] (Three View Geometry Program), using the measured trajectory projections in at least two views. The kinematic fitting to particular final state hypotheses is done by SQUAW.[8] The two programs are run as one unified program, known as SIOUX.

We used a beam averaging technique in SIOUX, as we know our beam momentum better than we can measure it on any event. For each event, a weighted average is taken of the measured curvature, with its error, and the median value for that beam momentum setting (swum to the event vertex), with its width. This width is determined from the width of the fitted momentum distribution, used in II.B above. It includes an intrinsic beam width of $\pm\frac{1}{2}\%$. The measured beam width is $\pm 1\%$, whereas the measurement uncertainties on any single event are no smaller than $\approx 2\%$ (and are usually less well determined). Thus we get a better determination of the beam momentum for each event, on the average.

Tracks with a projected length of less than 1 millimeter are difficult to see in bubble chamber photographs, and cannot be measured. There is often a low momentum proton (the spectator proton) in the final state of a $\pi^+ d$ interaction; protons with momentum less than 80 MeV/c have lengths less than 1 millimeter and are not visible. Since one positive charge is not seen, these events are odd-pronged. The momentum of these unseen protons, although unmeasured, is not unknown: we know it is less than about 90 MeV/c. The most probable value for the unseen spectator momentum is 40 MeV/c.

This distribution (given by the deuteron wave function) is approximated by using (0,0,0) ± (30,30,40) MeV/c for the measured momentum. If there are no missing particles, the resulting pseudo-four-constraint fit reproduces the expected spectator momentum distribution reasonably well. If there is one missing particle, one obtains a pseudo-one-constraint fit, which systematically underestimates the spectator momentum: at best, the fit can only determine the projection of the missing spectator momentum on the measured value for the overall missing momentum.

The density of the deuterium in the bubble chamber is needed to determine the range-momentum scale factor and the index of refraction of the liquid in the chamber; it has been determined from π-μ-e decays.[9]

E. Twice-failing Events

The 5- and 6-prong events which fail in SIOUX are re-measured, up to five times. Those events which failed twice were examined on the scan table by expert scanners, to find out why they were not fitting. Events which had been incorrectly called 5- and 6-prongs were reassigned to their correct topology; events which were not measurable (too many short tracks, too many kinks, too many scatters, vertex obscured) were not processed any further. This procedure was repeated after each measurement.

III. FINAL STATES AND THE SEPARATION OF HYPOTHESES

The 5- and 6-prong events were fitted to the following reactions:

$$\pi^+ d \rightarrow pp\pi^+\pi^+\pi^-\pi^- \quad (1)$$

$$\rightarrow pp\pi^+\pi^+\pi^-\pi^-\pi^o \quad (2)$$

$$\rightarrow pp\pi^+\pi^+\pi^-\pi^-\gamma \quad (3)$$

$$\rightarrow pp\pi^+\pi^+\pi^-\pi^-(MM > \pi^o\pi^o) \quad (4)$$

$$\rightarrow pn\pi^+\pi^+\pi^+\pi^-\pi^- \quad (5)$$

$$\rightarrow p\pi^+\pi^+\pi^+\pi^-\pi^-(MM > n\pi^o) \quad (6)$$

$$\rightarrow d\pi^+\pi^+\pi^+\pi^-\pi^- \quad (7)$$

$$\rightarrow \pi^+\pi^+\pi^+\pi^+\pi^-\pi^-(MM > nn) \quad (8)$$

where MM stands for missing mass. Reactions (7) and (8) were tried only for 6-prong events.

A. Selection of the Best Fit

We attempted to separate competing hypotheses, for events which fit more than one final state hypothesis, by using the formula

$$\text{Quality} = 5 \cdot N - \chi^2 , \quad (9)$$

where N is the number of constraints and χ^2 is calculated in the kinematic fit to the hypothesis. The hypothesis with the highest quality was then selected as the best fit for each event.

Equation (9) is an application of the following procedural rules:

a) if two ambiguous fits have different numbers of constraints, prefer the one with the higher number of constraints; and

b) if two ambiguous fits have the same number of constraints, choose the one with the lower χ^2 for its kinematic fit.

Procedure (a) is based on the belief that the larger the number of constraints, the more difficult it will be for the wrong hypothesis to look like a solution; and procedure (b) is equivalent to taking the hypothesis with the higher confidence level.

Initially 84% of our events fit more than one final state hypothesis. With the above criterion for the ordering of the fits, nearly half of the second-best fits were γ fits. If these second-best γ fits were ignored, only 45% of the events had more than one final state hypothesis.

B. Definition of Ambiguous Events

Equation (9) is statistical in nature, and a more detailed study of an event can result in a different choice for the best fit. In particular, one would like to look more closely at events for which the two best hypotheses have nearly the same quality. Thus we define an event to be ambiguous if the difference in quality values for the two best fits is less than 10; otherwise the best fit is called unambiguous.

Formulas other than equation (9) can be used, and all give somewhat different selections for the "best" fits. However, the ambiguous fits have been resolved where possible (see Section III.C below) and we have checked that the final selection of best fits is not sensitive to the exact form of equation (9).

C. Definition of Resolvable Ambiguities

The difference in bubble density for a π^+ and a proton at the same momentum provides our best criterion for resolving ambiguous fits; however, the 5- and 6-prong events do not have pulse-height measurements available, since they were measured on the Franckenstein measuring projectors. The bubble densities, and other information, can be checked if the event is examined on the scan table. It is seldom worth examining an event unless at least two of its fits are resolvable by their predicted bubble densities, however. Two fits are defined to be resolvable if the predicted bubble densities (relative to a minimum ionizing track) differ by 50% for at least one track. (We have found experimentally that one cannot reliably distinguish two bubble densities if they differ by less than 50%.)

The ambiguous events with resolvable fits were examined on the scan table, and ambiguities were resolved insofar as possible. After this ambiguity scan, we found that 31% of the events still had more than one fit (ignoring the second-best γ fits); however only 13% are ambiguous, using the definition given above.

D. Final Separation of Hypotheses

The remaining ambiguities are most serious between reactions (2) and (3). There are 728 events which fit both reactions as best or second-best, of which 678 are called ambiguous. We expect the γ events to result from η decays into $\pi^+\pi^-\gamma$. We can only see an η signal in the γ events if we look at a selected sample of unambiguous events, and then only $\approx$20% are η events. The separation by equation (9) is not right, as we then see a clear ω signal in the $\pi^+\pi^-\gamma$ spectrum, shifted down by $\approx$30 MeV, as well as an η peak, shifted down by $\approx$50 MeV. This false η peak (from $\eta \to \pi^+\pi^-\pi^o$ events) also makes it difficult to see the real $\eta \to \pi^+\pi^-\gamma$ peak.

Since the γ and π^o hypotheses cannot be resolved, we take the π^o fit in cases where these two are ambiguous. Since the real γ events (from $\eta \to \pi^+\pi^-\gamma$) are similar to π^o events (from $\eta \to \pi^+\pi^-\pi^o$), this mainly results in broadening the η peak.

There are 1667 events remaining in which reaction (3) is second-best to reaction (1); however, only 361 are ambiguous. (Reaction (1) can only be ambiguous with reaction (3) if it has a confidence level less than 30%.) This sample of γ events shows no η peak, and an upper limit of 14 excess events in the region of the η', over 35 background events. This gives a rough estimate that no more than $\approx$144 of these events can be real γ events. We would see 36 events involving a real $\eta \to \pi^+\pi^-\gamma$ decay, as a three standard deviation effect. There is no excess of events in this

region of $(\pi^+\pi^-\gamma)$ mass, and we conclude that there are less than 12 γ events with a 68% confidence level. Since in fact, for all ambiguous events reaction (1) is called best, we resolve the ambiguity by disregarding the second-best γ fits.

Most of the other ambiguities involve the missing mass reactions (4) and (6), and little can be done with them. The largest remaining ambiguity involves 10 events ambiguous between reactions (1) and (2), which amounts to about 1% of reaction (2).

We have used a program which simulates the measuring and fitting process for each final state, to check our understanding of the ambiguities. The results of the program predict the ambiguities mentioned above, such as between reactions (1) and (3), and reactions (2) and (3). The results also indicate that there should be little ambiguity between reactions (1) and (2), which is indeed what we find. However, the results do show serious ambiguities between reactions (2) and (5), because one of the $n\pi^+$ combinations can often be re-interpreted as a $p\pi^o$. We do not observe this ambiguity in our events, as this is exactly the sort of ambiguity which is successfully resolved by the ambiguity scan.

We have done a special check of this, by looking at 50 events which had any fits to reaction (5). This study yields the estimate that 1/44 of the events truly belonging to reaction (5) are called reaction (2), which is not a significant amount of contamination.

The final separation of events into reactions (1) to (8) is given by beam momentum in Table 3. The systematic errors due to the separation are estimated to be less than the statistical errors, in most cases.

Table 3. Number of events assigned to final states, by beam momentum.

Final State	Beam Momentum (GeV/c)							
	1.10	1.30	1.53	1.58	1.70	1.86	2.15	2.37
$pp\pi^+\pi^+\pi^-\pi^-$	2	11	132	36	352	497	922	334
$pp\pi^+\pi^+\pi^-\pi^-(\pi^o \text{ or } \gamma)$			21	5	71	159	411	186
$pp\pi^+\pi^+\pi^-\pi^-(MM > \pi^o\pi^o)$			1		3	11	26	6
$pn\pi^+\pi^+\pi^+\pi^-\pi^-$			3		16	34	119	57
$p\pi^+\pi^+\pi^+\pi^-\pi^-(MM > n\pi^o)$					2	6	22	12
$d\pi^+\pi^+\pi^+\pi^-\pi^-$							2	
$\pi^+\pi^+\pi^+\pi^+\pi^-\pi^-(MM > nn)$						1	1	

IV. CROSS SECTIONS

The cross section σ for a reaction can be found from the number of events N_{total} which are a result of this reaction and the pathlength L, from the formula

$$\sigma = N_{total}/L \ , \qquad (10)$$

where σ is in μb if the pathlength is in events/μb. The pathlengths in this experiment are given in Table 1.

The total number of events is seldom known: the scanners miss some events. This is taken into account by correcting the observed number of events N by the scanning efficiency S. The scanning efficiency is the ratio of the number of events found by the scanners to the number of events that are actually on the film. It can be estimated by re-scanning part of the film and comparing results. The scanning efficiency was checked for the 3- and 4-prong events[10] and estimated to be 95% . A check scan has not been done for the 5- and 6-prong events; we use 95% , which should be within 5% of the true value. The systematic error in the cross sections due to S is estimated to be $\leq 5\%$.

A. Deuteron Cross Sections

In this section we discuss the calculation of the cross sections for reactions (1) to (6). The corrections to the number of fitted events are discussed, and the cross section calculation described.

The first correction to the number of events is for the scanning efficiency, as discussed above. The second correction is for the passing rate R. The passing rate is the fraction of valid events scanned which have been successfully fit to one of the final state hypotheses. (Events which did not fit were re-processed, as discussed in Section II.) The passing rates are given for each beam momentum in Table 4.

The sample of 3461 fitted events contains 75 events which have beam azimuth or dip angles outside the beam fiducial region (suggesting that they have scattered and lost energy somewhere), and 140 events where the beam entered through the chamber walls, rather than through the entrance window. There are 52 events which we reject because their production vertices are not in the required fiducial volume. These 267 events have been removed from the sample of fitted events.

Similarly, fitted events with very low confidence levels contain most of the events on which the measurer has made a serious mistake (measuring through a scatter, for example). (The confidence level distributions for the fitted reactions are flat, except at confidence levels $< 4\%$, where there is a peaking of events. Because these low-confidence level events could belong to any reaction, we remove most of the excess (135 events) by requiring that the confidence level for the fit be greater than 1%.

Some events suffer a reduction in constraints because some quantity cannot be measured, e.g., the momentum of a short pion

Table 4. The 5- and 6-prong passing ratios.

Beam Momentum (GeV/c)	5-prongs	6-prongs	Both
1.10	0.5	1.	0.7
1.30	1.	1.	1.
1.53	0.87	0.95	0.92
1.58	0.88	0.90	0.89
1.70	0.91	0.94	0.93
1.86	0.96	0.93	0.94
2.15	0.92	0.92	0.92
2.37	0.96	0.92	0.94

track. All constraint-reduced events (136 in number) have been removed from the sample. The effect of these cuts is to remove a fraction 1-C of the events. We call **C** the cut correction factor.

For the remainder of this paper we will consider only events satisfying these cuts.

The cross section for each final state is then calculated as

$$\sigma_f = N_f/(L \cdot R \cdot S \cdot C), \tag{11}$$

where N_f is the remaining number of events in the final state. The number of events, N_f, and the cut correction factor C are tabulated in Table 5. The π^o and γ final states are combined. The resulting cross sections are given in Table 6. The quoted errors have a ±6% systematic uncertainty folded in with the statistical errors and the pathlength errors.

B. Nucleon Cross Sections

1. The Spectator Model

The interaction of the incident pion with the deuteron can be described simply in this way: At incident pion momenta of 1-2 GeV/c, the de Broglie wavelength of the pion in a π-nucleon c.m. frame is 0.4 to 0.2 fermi. Thus, as the nucleons in the deuteron are loosely bound, with a binding energy of 2.2 MeV, and are typically ≈ 3 fermis apart, the pion should interact with the nucleons singly, rather than together. When the pion interacts with only one nucleon, the other proceeds with its original momentum, merely a spectator to the interaction.

Table 5. Number of events, after cuts (see text).

Final State	Beam Momentum (GeV/c)							
	1.10	1.30	1.53	1.58	1.70	1.86	2.15	2.37
$pp\pi^+\pi^+\pi^-\pi^-$	2	10	113	33	311	438	768	266
$pp\pi^+\pi^+\pi^-\pi^-(\pi^o \text{ or } \gamma)$			16	4	61	134	345	152
$pp\pi^+\pi^+\pi^-\pi^-(MM > \pi^o\pi^o)$			1	0	3	10	20	5
$pn\pi^+\pi^+\pi^+\pi^-\pi^-$			3	0	14	26	103	42
$p\pi^+\pi^+\pi^+\pi^-\pi^-(MM > n\pi^o)$					2	5	21	11
Cut factor	1.	0.9	0.85	0.90	0.88	0.87	0.84	0.80

Table 6. Cross sections for $\pi^+ d$ reactions.

Final State	Beam Momentum (GeV/c)							
	1.10	1.30	1.53	1.58	1.70	1.86	2.15	2.37
$pp\pi^+\pi^+\pi^-\pi^-$	7 ± 5	26 ± 8	60 ± 7	101 ± 20	132 ± 12	194 ± 17	339 ± 27	443 ± 55
$pp\pi^+\pi^+\pi^-\pi^-(\pi^o$ or $\gamma)$			9 ± 2	12 ± 6	26 ± 4	59 ± 7	152 ± 13	253 ± 34
$pp\pi^+\pi^+\pi^-\pi^-(MM > \pi^o\pi^o)$			1 ± 1	-	1 ± 1	4 ± 1	9 ± 2	8 ± 4
$pn\pi^+\pi^+\pi^+\pi^-\pi^-$			2 ± 1	-	6 ± 2	11 ± 2	45 ± 5	70 ± 13
$p\pi^+\pi^+\pi^+\pi^-\pi^-(MM > n\pi^o)$					1 ± 1	2 ± 1	9 ± 2	18 ± 6

The spectator model says that the spectator nucleon should have a distribution in momentum given by the deuteron wave function. We will use the Hulthén wave function to approximate the deuteron wave function.[11] (See Appendix A for the explicit form of the Hulthén wave function.) Since the nucleons in the deuteron have no orientation with respect to the beam, the spectator model is often said to predict that the spectator nucleons should be distributed uniformly in the lab. (I.e., the cosine of the angle between the spectator and the beam should have a flat distribution, and there should be no dependence on the angle around the beam.)

The distribution of the cosine of the angle between the spectator and the beam is not expected to be flat, due to two effects:

a) there is a higher flux of particles when the beam and target collide head-on, and

b) a rapid increase (decrease) of the reaction cross section with energy preferentially selects forward (backward) spectators.

These effects will now be discussed.

The Fermi motion of the target nucleon varies the density of nucleons in the target (due to the relativistic length contraction), as well as the beam-target relative velocity. An invariant expression for the flux of particles (thus defining an invariant cross section) is

$$\text{Flux}(\vec{p}_b, \vec{p}_t) = \sqrt{(P_b \cdot P_t)^2 - m_b^2 m_t^2}\,/m_b m_t \qquad (12)$$

(the Møller flux factor[12]), where P_b and P_t are the respective four-vectors for the beam and target, and m_b, m_t are their respective masses. The flux factor reduces to

$$\text{Flux} = \rho_b \rho_t \left|\vec{v}_b - \vec{v}_t\right|$$

whenever $\vec{v}_b \parallel \vec{v}_t$. Here ρ_b, ρ_t are the beam and target particle densities and $\vec{v}_b$, $\vec{v}_t$ are their respective velocities.

If the Hulthén wave function is H(p), the number of reactions with a beam-target cosine equal to $x \pm dx/2$ is

$$dN = dx\ \text{Const.} \int \text{Flux}(p_b, p_t, x) \cdot \sigma(E_{c.m.}) \cdot |H(p_t)|^2 p_t^2 dp_t \qquad (13)$$

where p_b, p_t are the magnitudes of the beam and target momentum. Note that $\vec{p}_{\text{spectator}} = -\vec{p}_t$, so that $x_{\text{spectator}} = -x$. The c.m. energy for the reaction is

$$E_{c.m.} = \sqrt{(P_b + P_t)^2}\ .$$

Since the flux factor is larger when $x = -1$ than when $x = +1$, we get result (a) stated above; and since $E_{c.m.}$ is larger when $x = -1$ than when $x = +1$, we get result (b) stated above. For $p_b = 1.9$ GeV/c the flux factor produces a 9% variation in the angular distribution, between $x = +1$ and $x = -1$. As we will see, the cross section dependence can produce much larger variations.

If the spectator model describes the data, then one can calculate πN cross sections from πd reactions, since the π really does scatter from only one nucleon. The calculation of the πN cross sections should be done by extrapolating the data to the free nucleon ($p_{spectator} \rightarrow 0$ almost puts the nucleons on their mass shells): however, when p_t = 250 MeV/c, the mass of the nucleon is only $\approx 3\%$ below its free-nucleon value, and this extrapolation can usually be ignored.

There are two effects which affect cross section determinations in deuterium which have not been discussed. These are the Glauber (screening) correction, and the suppression of certain momentum states by the Pauli Exclusion Principle (which affects only the non-spin flip amplitude). These effects are too small to be of any importance in this study; see, however, the discussion in ref. 1.

Within the framework of the spectator model, we can determine the nucleon cross sections as a function of the c.m. energy by observing the number of events in a final state at $E_{c.m.} = E$, within ΔE, compared to the pathlength which the spectator model assigns to this interval of $E_{c.m.}$. The distribution of the pathlength in $E_{c.m.}$, according to the spectator model, is discussed in detail in Appendix A. Figure 2 illustrates the distribution of pathlength calculated for the 1.86 GeV/c beam setting.

If an event is the result of a reaction involving both nucleons, however, we can no longer count the event in the spectator model. For each momentum setting, these events are removed.

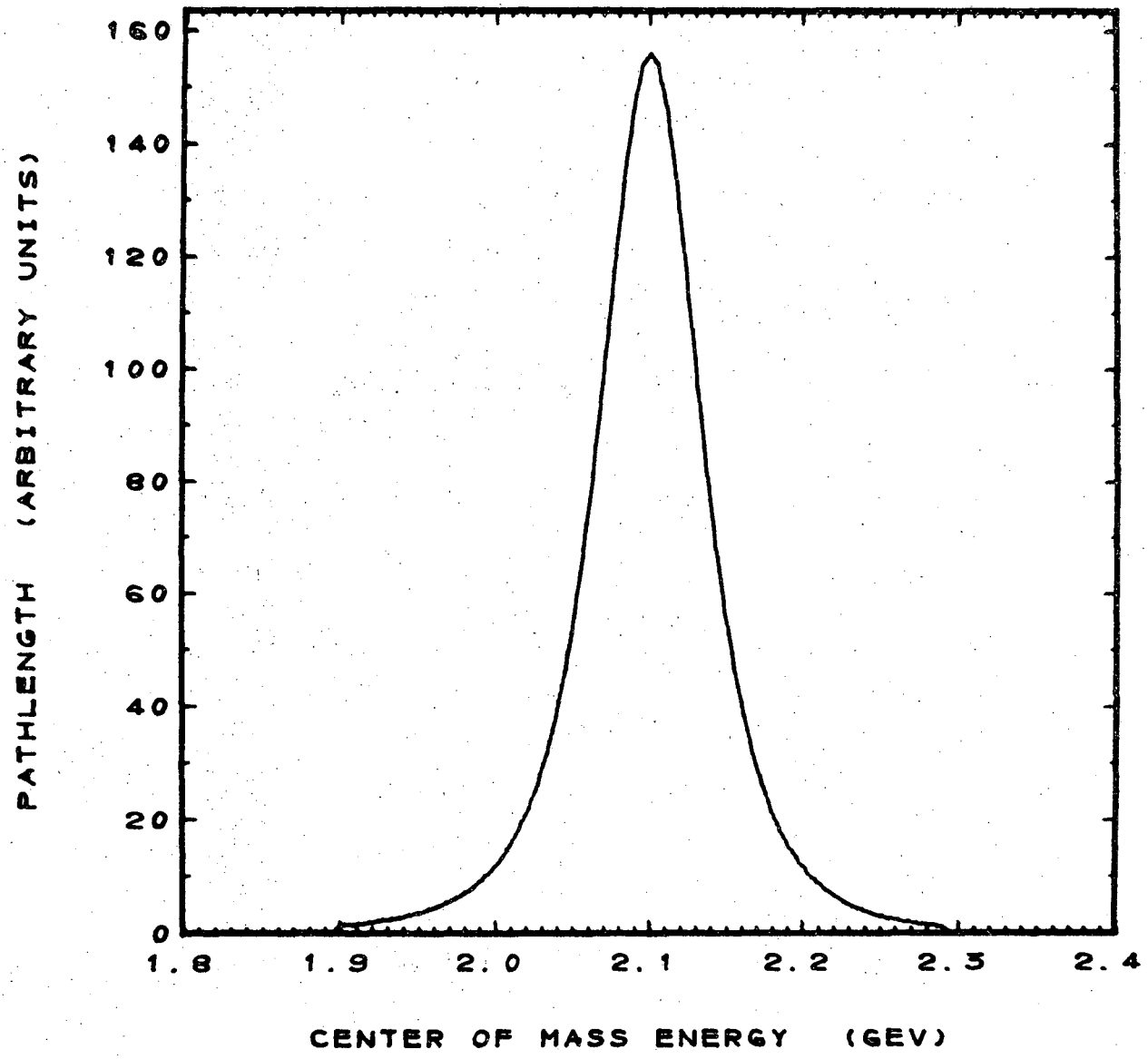

Figure 2. Distribution of pathlength in c.m. energy for a beam momentum of 1.86 GeV/c.

If we assume that all of these reactions are actually a result of multiple scattering, rather than to simultaneous interaction with both nucleons, then there is a first πN interaction at a unique $E_{c.m.}$, followed by an elastic (or charge-exchange, where possible) re-scattering of one of the final state particles on the other nucleon. Thus a correction must be applied to find the πN cross section (see below).

2. Comparison of Data with Spectator Model

Figure 3 shows the spectator momentum distribution for all events from reaction (1), which is a four-constraint fit. The curve is the spectator model prediction, normalized to fit the data below 250 MeV/c. The fraction of events with spectator momentum over 250 MeV/c is 34%. The nucleons in the deuteron have a Fermi momentum greater than 250 MeV/c only 2-7% of the time (the number is not well known), so it is clear that the high momentum spectators are not spectators to the scattering at all--both nucleons have been struck. We require that the spectator momentum be less than 250 MeV/c when using the spectator model to obtain πN cross sections. There is quite reasonable agreement between the data and the curve below 250 MeV/c. For the remainder of this paper we will consider only events satisfying this condition.

The angular distribution of the spectator proton with respect to the beam is compared with the prediction of the spectator model

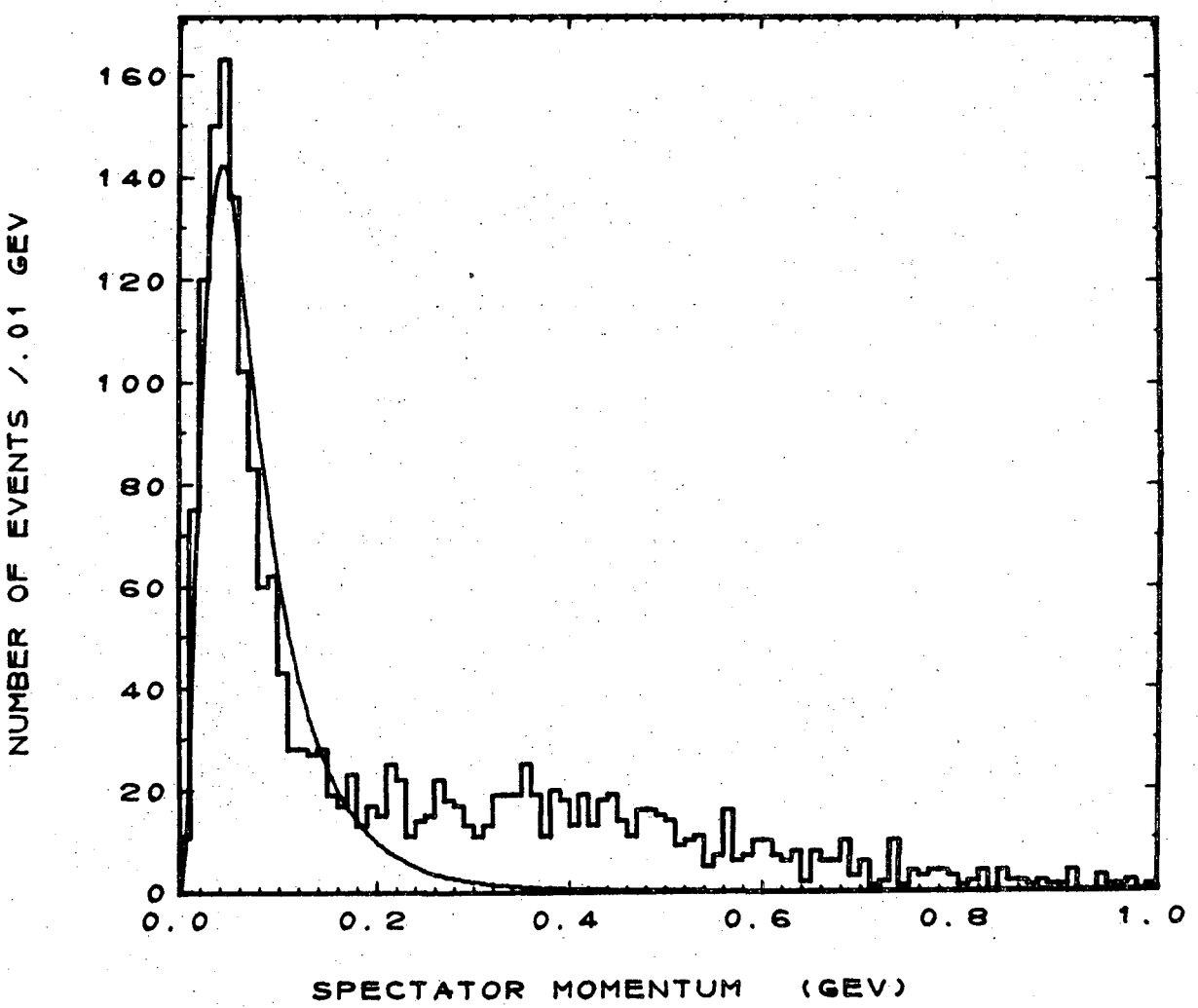

Figure 3. Spectator momentum distribution compared to the prediction of the spectator model, for 1936 events assigned to reaction (1).

in Figure 4. The curve is the spectator model prediction, as given in equation (13), with an additional sum over beam momenta. The cross sections determined below for reaction (1) were used in the integral. The curve and the histogram agree with a 7% confidence level. This sample of events is consistent with the spectator model.

3. Calculation of the Nucleon Cross Sections

The number of events assigned to each reaction (1) to (5) has been tallied by c.m. energy for each final state. These numbers are given in Table 7. The c.m. energy is defined to be

$$E_{c.m.} = \sqrt{(P_b + P_d - P_s)^2} \quad ,$$

where P_d is the deuteron four-vector, and P_s is the spectator four-vector. This four-vector sum is equal to the sum of all the four-vectors for the final-state particles, minus the spectator. The events removed from the sample by the spectator cut at 250 MeV/c have been tallied for each final state at each momentum setting, and are shown in Table 8.

We need to know the correction for high spectator momentum events for each c.m. energy bin (for each final state). To find this we distribute all the events at each beam momentum according to the pathlength (see Appendix A and Figure 2); the same process is applied to the number of high spectator momentum events (Table 8). The fraction of high spectator momentum events can then be

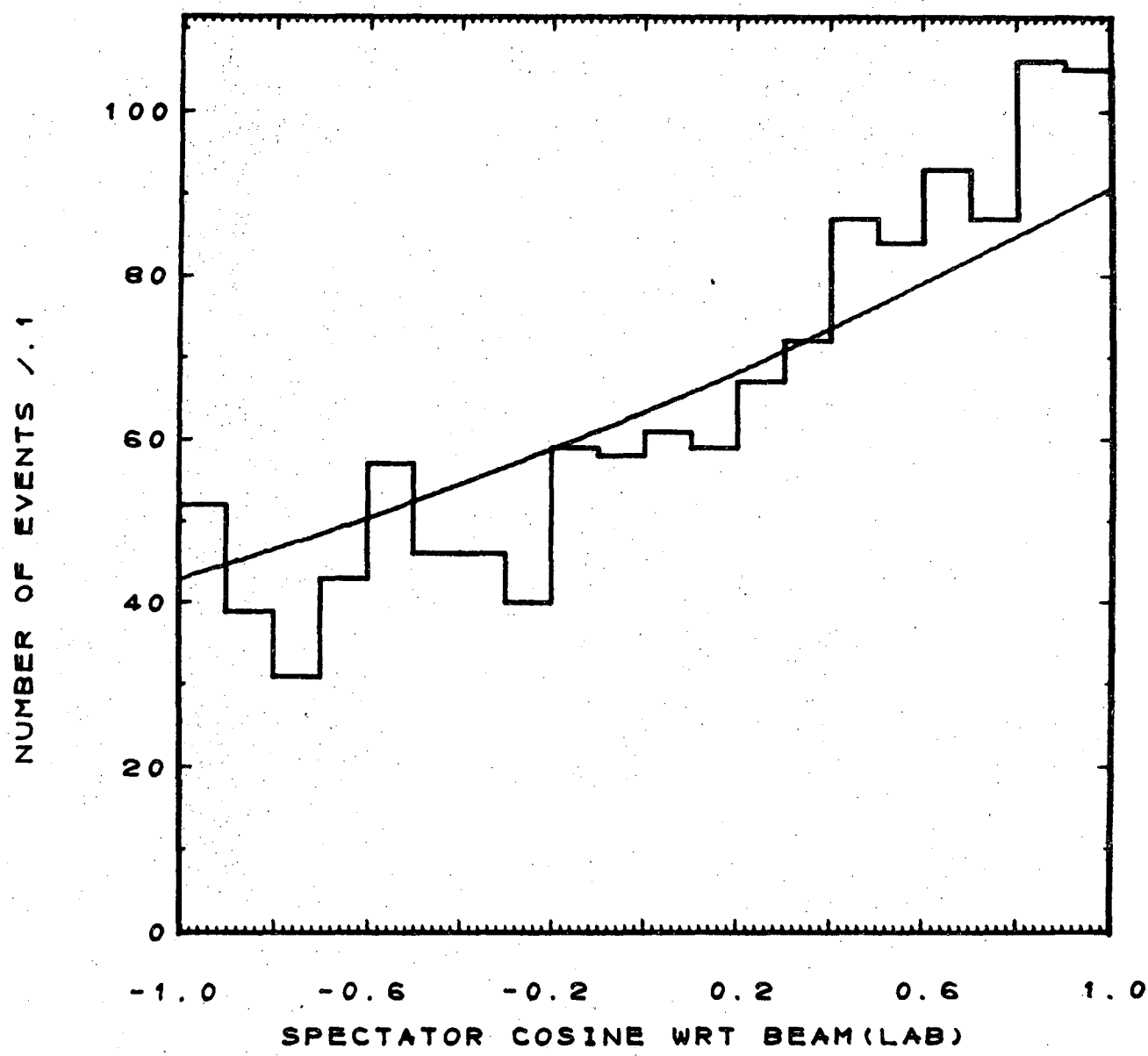

Figure 4. Spectator cosine distribution compared to the spectator model prediction (including the cross section effect), for 1292 events assigned to reaction (1), with spectator momentum less than 250 MeV/c.

Table 7. Number of events by c.m. energy (spectator momentum less than 250 MeV/c).

Final State	Center of Mass Energy (GeV)						
	1.73	1.84	1.94	2.02	2.11	2.22	2.33
$p\pi^+\pi^+\pi^-\pi^-$	2	9	70	179	305	485	234
$p\pi^+\pi^+\pi^-\pi^-(\pi^o \text{ or } \gamma)$			11	39	81	188	125
$p\pi^+\pi^+\pi^-\pi^-(MM > \pi^o\pi^o)$				3	3	6	6
$(p \text{ or } n)\pi^+\pi^+\pi^+\pi^-\pi^-$ [a]			1	3	13	41	29

[a] The non-spectator nucleon can be either a proton or a neutron.

Table 8. Number of events by beam momentum with spectator momenta above 250 MeV/c.

Final State	Beam Momentum (GeV/c)							
	1.10	1.30	1.53	1.58	1.70	1.86	2.15	2.37
$pp\pi^+\pi^+\pi^-\pi^-$	1	4	43	17	121	153	251	58
$pp\pi^+\pi^+\pi^-\pi^-(\pi^o \text{ or } \gamma)$			5	1	25	49	132	49
$pp\pi^+\pi^+\pi^-\pi^-(MM > \pi^o\pi^o)$			1			8	10	2
$pn\pi^+\pi^+\pi^+\pi^-\pi^-$					11	14	52	23

calculated for each c.m. energy bin; these fractions are given in Table 9.

This procedure yields the probability of a re-scattering, averaged over the c.m. energy bin; if either the cross section or this probability are constant over the c.m. energy bin, we get the right correction factor in this way.

The cross sections, corrected for the cut on high spectator momentum events, have been calculated and are shown in Table 10. Reaction 5 has a neutron spectator 59% of the time, averaged over all c.m. energies; the cross section given is the sum of the $\pi^+ n \to n\pi^+\pi^+\pi^+\pi^-\pi^-$ and $\pi^+ p \to p\pi^+\pi^+\pi^+\pi^-\pi^-$ cross sections.

Our determination of the $\pi^+ n \to p\pi^+\pi^+\pi^-\pi^-$ cross section is shown in Figure 5. The charge symmetric data for the reaction $\pi^- p \to n\pi^+\pi^+\pi^-\pi^-$ is also shown; this data is a compilation from many experiments.[13] Our data determines the cross section over most of our c.m. energy range.

Table 9. Fraction of events lost to high momentum spectator events, by c.m. energy.

	Center of Mass Energy (GeV)						
Final State	1.73	1.84	1.94	2.02	2.11	2.22	2.33
$p\pi^+\pi^+\pi^-\pi^-$	0.46	0.40	0.40	0.39	0.35	0.32	0.25
$p\pi^+\pi^+\pi^-\pi^-(\pi^o$ or $\gamma)$	0.3	0.3	0.34	0.39	0.37	0.38	0.34
$p\pi^+\pi^+\pi^-\pi^-(MM > \pi^o\pi^o)$	0.9	0.8	0.7	0.4	0.7	0.51	0.44
$(p$ or $n)\pi^+\pi^+\pi^+\pi^-\pi^-$	0.	0.2	0.3	0.69	0.55	0.51	0.54

Table 10. Nucleon cross sections in μb.

Final State	Center of Mass Energy (GeV)						
	1.73	1.84	1.94	2.02	2.11	2.22	2.33
$p\pi^+\pi^+\pi^-\pi^-$	13 ± 9	32 ± 11	59 ± 8	124 ± 13	198 ± 19	337 ± 29	429 ± 49
$p\pi^+\pi^+\pi^-\pi^-(\pi^o \text{ or } \gamma)$			8 ± 3	27 ± 5	54 ± 7	142 ± 15	259 ± 34
$p\pi^+\pi^+\pi^-\pi^-(MM > \pi^o\pi^o)$				2 ± 1	4 ± 2	6 ± 2	15 ± 6
$(p \text{ or } n)\pi^+\pi^+\pi^+\pi^-\pi^-$			1 ± 1	4 ± 2	12 ± 4	39 ± 7	86 ± 18

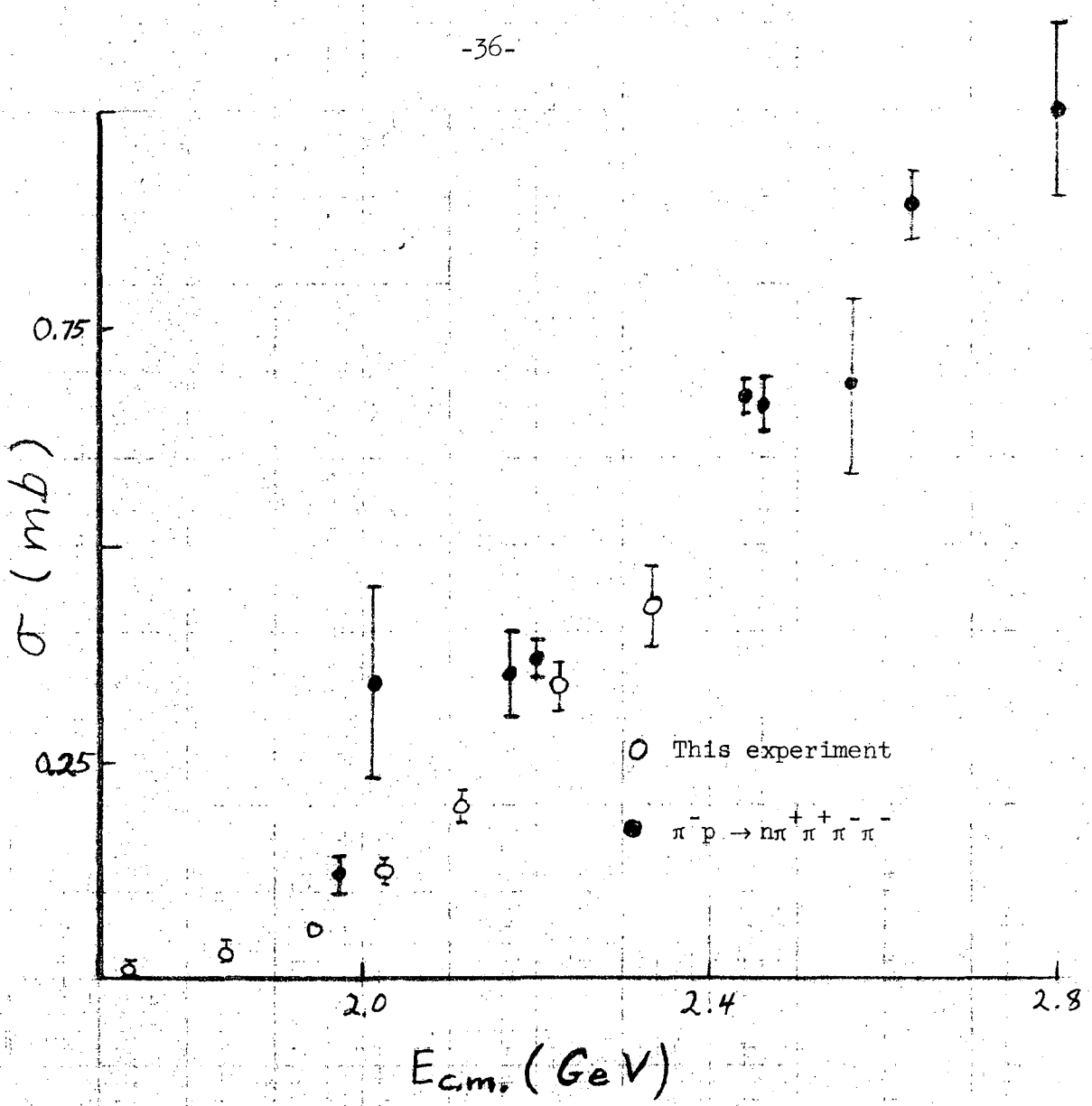

Figure 5. Cross section for $\pi^+ n \to p\pi^+\pi^+\pi^-\pi^-$, and charge-symmetric data.[13]

V. η' PRODUCTION

A. Known Properties of the η' Meson

The η' meson (also known as the X^o or η^*) was first discovered in K^-p experiments in 1964.[17,18] Its quantum numbers are $I^GJ^P = 0^+0^-$.[19,20] The η' decays into the state $\pi\pi\eta$ 71% of the time.[20] Using the known neutral-to-charged branching ratio of the η meson,[20] and the fact that the $(\pi\pi)_{I=0}$ state is $\pi^+\pi^-$ 2/3 of the time, the branching ratios of the η' into the various final states are found to be

$$\eta' \rightarrow \pi^+\pi^-(\eta,\ \eta \rightarrow \text{neutrals})\ (34\%) \tag{14}$$

$$\rightarrow \pi^+\pi^-(\eta,\ \eta \rightarrow \pi^+\pi^-\pi^o \text{ or } \pi^+\pi^-\gamma)\ (14\%) \tag{15}$$

$$\rightarrow \pi^o\pi^o(\eta,\ \eta \rightarrow \pi^+\pi^-\pi^o \text{ or } \pi^+\pi^-\gamma)\ (7\%)$$

$$\rightarrow \pi^+\pi^-\gamma\ (22\%)$$

$$\rightarrow (\text{neutrals})\ (23\%)$$

The η' has also been observed in the reactions $\pi^+p \rightarrow \Delta^{++}\eta'$,[21] $\pi^-p \rightarrow n\eta'$,[22,23] and $\pi^+d \rightarrow pp\eta'$.[24,25,26,27] The amplitudes for the reactions $\pi^-p \rightarrow n\eta'$ and $\pi^+n \rightarrow p\eta'$ should be equal, by the charge-symmetry of strong interactions.

B. η' Production in 5- and 6-prong Events

The final state $pp\pi^+\pi^+\pi^-\pi^-(\pi^o \text{ or } \gamma)$ has been studied for evidence of η' production in π^+d interactions. The small number of events preferring the hypothesis with a γ in the final state

are included with the π^o events. (See Section III for a discussion of the separation of hypotheses.)

The scatterplot of the "spectator" proton momentum versus the $(\pi^+\pi^+\pi^-\pi^-\pi^o)$ mass is shown in Figure 6. The η' signal is at a mass of 0.96 GeV/c^2; most of the η' events have reasonable spectator momenta--only 15% have spectator momenta over 0.25 GeV/c. Since we are particularly interested in the process $\pi^+ n \to p\eta'$, only events with proton spectator momentum less than 0.25 GeV/c are considered, and the spectator model is used to infer the interaction on a free neutron.

The evidence for η' production in this final state is summarized by the scatterplot of the $(\pi^+\pi^-\pi^o)$ mass (all four combinations are plotted) versus the $(\pi^+\pi^+\pi^-\pi^-\pi^o)$ mass. This plot is shown in Figure 7. The correlation of η and η' events is quite striking. The scatterplot of c.m. energy versus the $(\pi^+\pi^+\pi^-\pi^-\pi^o)$ mass is shown in Figure 8, together with its mass projection. The η' signal at a mass of 0.96 GeV/c^2 is very clear, with no more than 20% background.

The scatterplot of c.m. energy versus the $(\pi^+\pi^-\pi^o)$ mass is shown in Figure 9, together with the $(\pi^+\pi^-\pi^o)$ mass projection. There is a strong η signal here, much more than be accounted for by η' decays alone.

The amount of η' production was determined by estimating background and counting events in the η' and η peaks. Every event

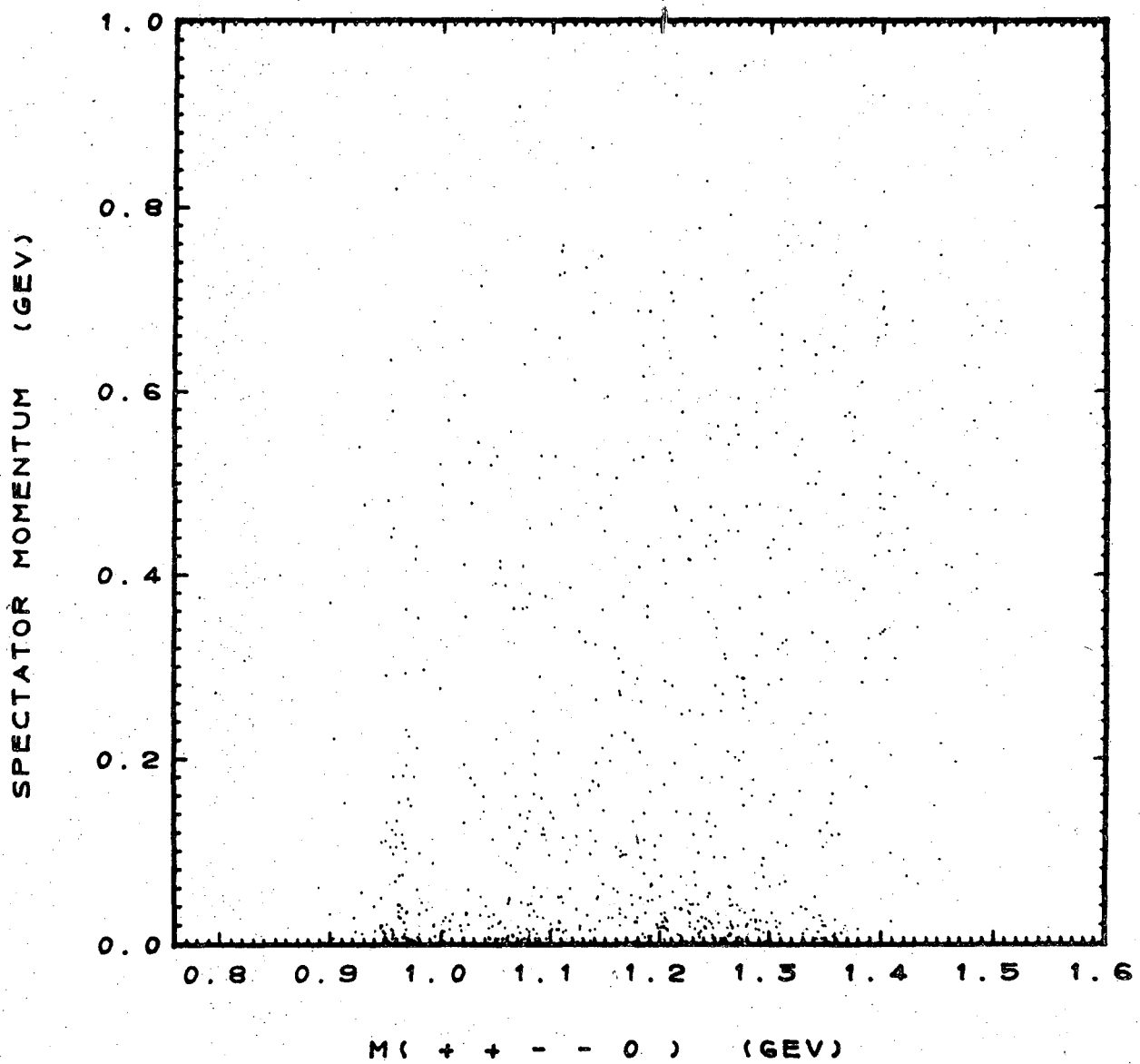

Figure 6. Spectator momentum versus $M(\pi^+\pi^+\pi^-\pi^-\text{neutral})$ where the neutral is a π^0 or γ (712 events).

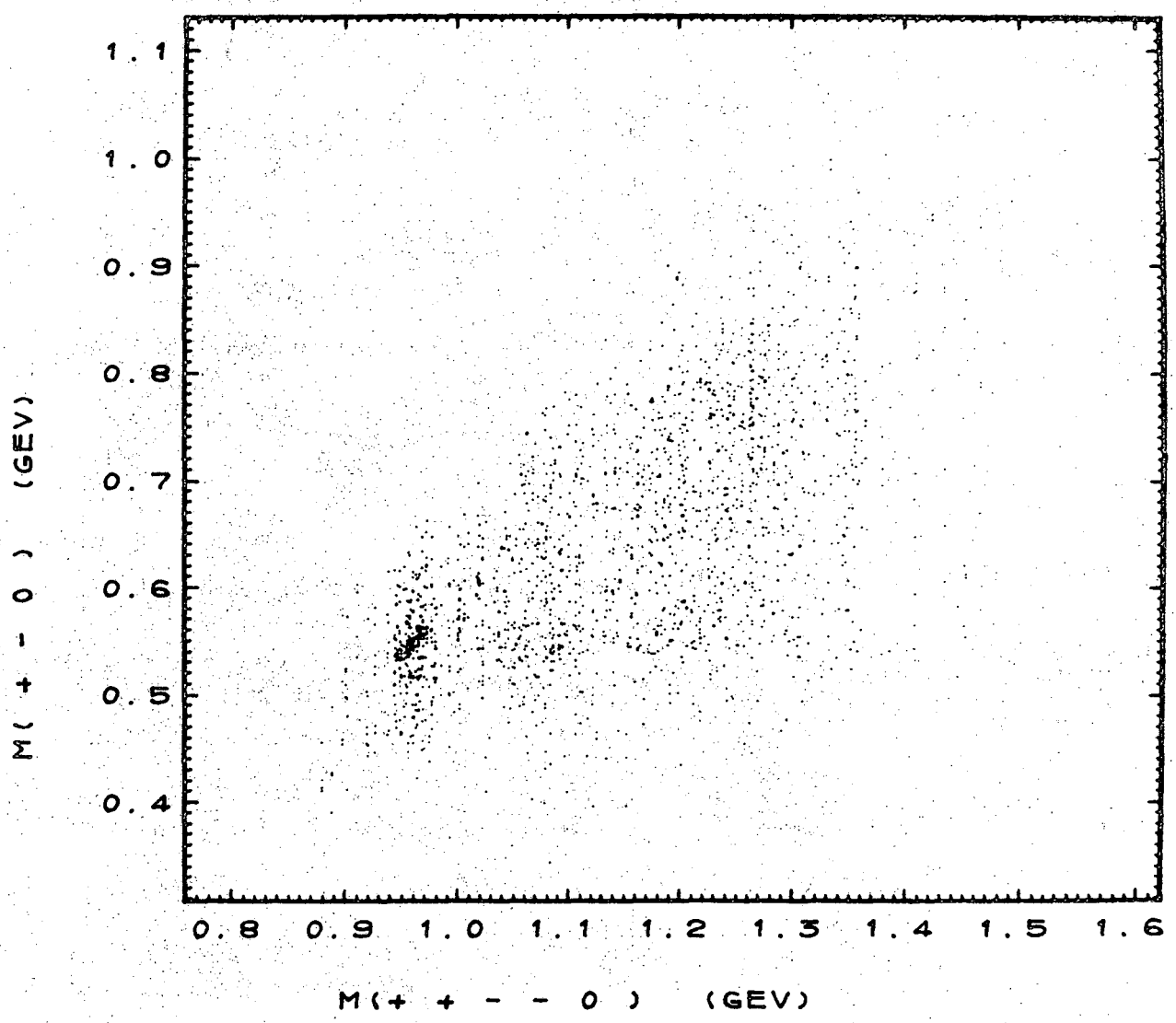

Figure 7. $M(\pi^+\pi^-\text{neutral})$ vs. $M(\pi^+\pi^+\pi^-\pi^-\text{neutral})$ where the neutral is a π^o or γ (4 combinations, 451 events).

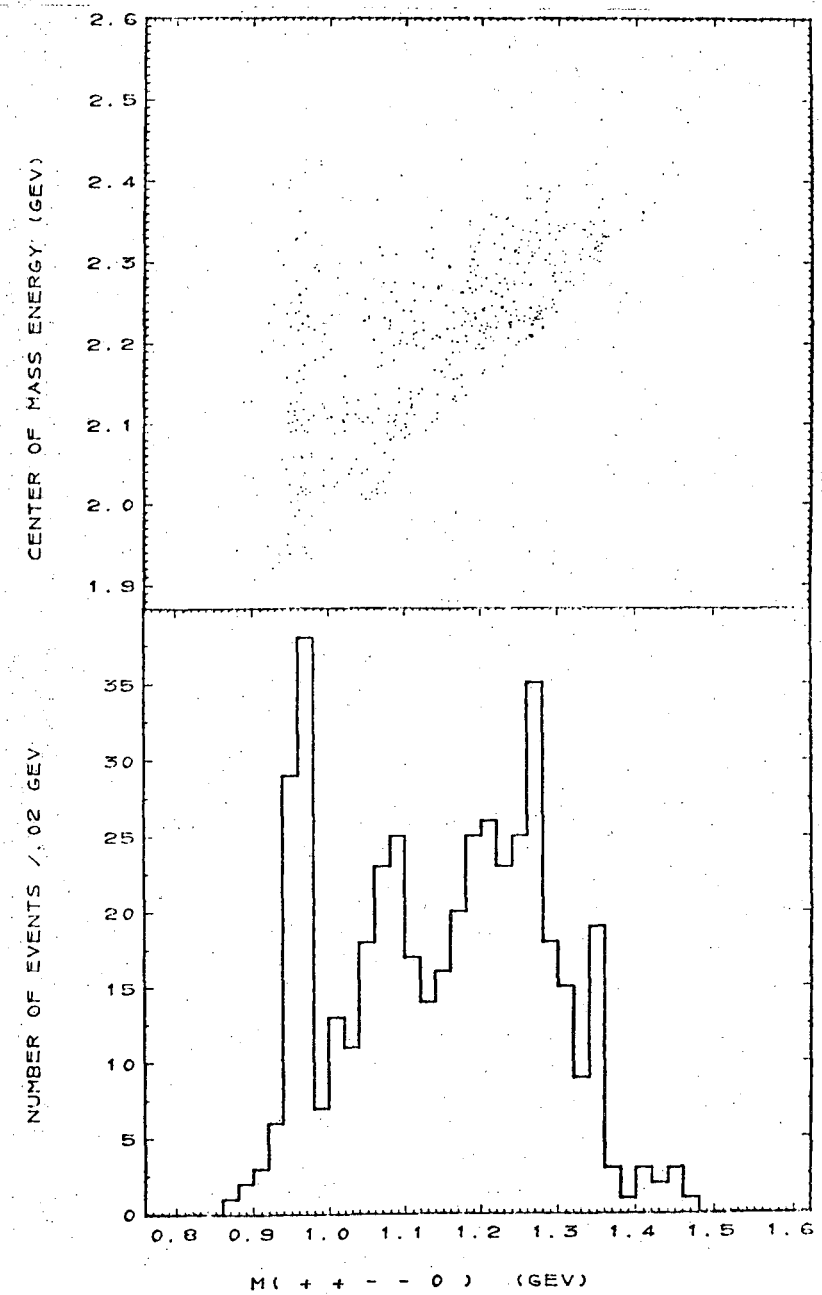

Figure 8. C. m. energy vs. $M(\pi^+\pi^+\pi^-\pi^-\text{neutral})$, with projection, where the neutral is a π^0 or γ (451 events).

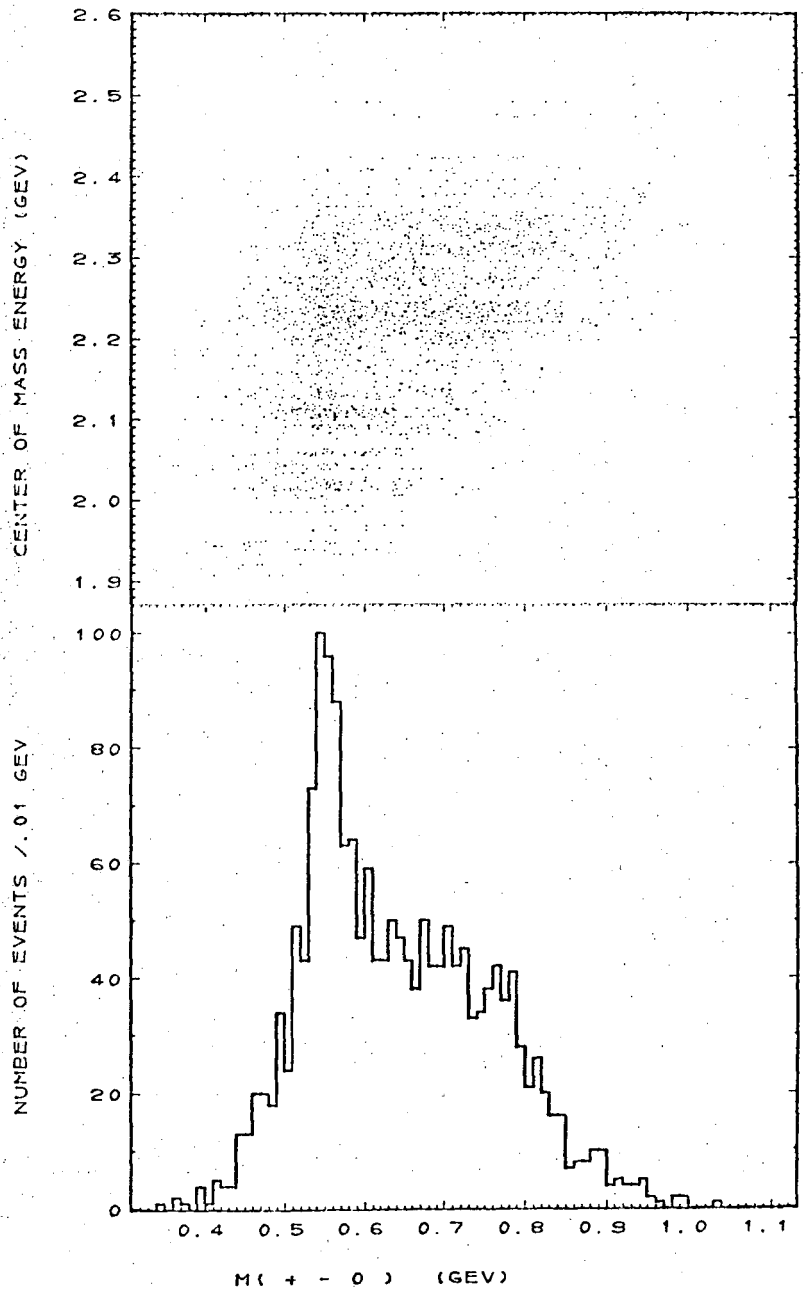

Figure 9. C. m. energy vs. $M(\pi^+\pi^-\text{neutral})$, with projection where the neutral is a π^0 or γ (4 combinations, 451 events).

in the η' region has at least one associated $(\pi^+\pi^-\pi^o)$ combination in the region of the η. The results have been verified by a maximum-likelihood fitting program; the agreement is very good.

The amount of η' at threshold requires special discussion, however. It turns out that when the c.m. energy is just above η' threshold, at $E_{c.m.} = 1.94$ GeV, then five pion phase space peaks at a mass of 960 MeV/c^2, with a width of 90 MeV/c^2. Also, when the five pion mass is 960 MeV/c^2, three pion phase space peaks at a mass of 550 MeV/c^2 (the η mass), with a width of 140 MeV/c^2. There are only 11 events in this region, so that background and resonance estimates difficult. The lower and upper bounds for the amount of η' production (by eye) are 0 and 75%; the maximum likelihood fit gives 0.36 ± 0.16 (the errors need not have come out symmetric).

The amount of η' production is shown as a function of c.m. energy in Table 11. The c.m. energy calculated for an event depends on the spectator momentum; since the spectator momentum for one-constraint odd-pronged events is systematically low (see Section II.D), their c.m. energies are systematically too close to the median c.m. energy for a given beam momentum setting. To avoid uncertainties due to the incorrectly determined c.m. energies, the c.m. energy bins were chosen to center on the median value for each beam momentum setting. Thus these events are assigned to the correct bin, even if their c.m. energy is not correctly determined.

Table 11. Amount of η' production (in %), by c.m. energy.

$E_{c.m.}$ (GeV)	1.94	2.03	2.11	2.22	2.33
Amount	35 ± 20	44 ± 13	26 ± 6	10 ± 2	4 ± 2

Table 12. η' production cross section in μb.

$E_{c.m.}$ (GeV)	1.94	2.03	2.11	2.22	2.33
$\sigma_{observed}$	3 ± 2	12 ± 4	14 ± 4	14 ± 3	10 ± 5
σ_{total}	21 ± 14	87 ± 30	103 ± 27	104 ± 24	76 ± 39

Table 13. Number of η' events.

$E_{c.m.}$ (GeV)	1.94	2.03	2.11	2.22	2.33
3-prong	6	-	-	43	18
4-prong	5	2	24	9	3
Both	11	-	-	52	21
5-, 6-prongs	4	13	17	17	5
Ratio	2.8 ± 1.6	-	-	3.1 ± 0.85	4.2 ± 2.1

The cross section for the reaction $\pi^+ n \to p\eta'$ was determined by using the results of Section IV.B for this final state. The detected η' cross section is given in Table 12. The total cross section for η' production can be found by using equation (15): we detect 14% of the η' events in this final state. The total η' production cross section is also given in Table 12. The summary of present data on η' production in $\pi^+ n$ interactions is shown in Figure 10, as a function of c.m. energy. Data for the charge-symmetric reaction are also shown in Figure 10.[28]

The production angular distribution for events in the η' mass region, 0.94 to 0.98 GeV/c^2, is shown in Figure 11. The distribution is flat near threshold, but develops forward peaking at higher energies. Figure 10 suggests that the reaction $\pi^+ n \to N^*_{1/2}(2190) \to p\eta'$ may account for most of the η' mesons produced in this experiment (the $N^*_{1/2}(2190)$ is 0.3 GeV/c^2 wide); however we expect a symmetric, sharply peaked angular distribution if we have pure resonance production. Figure 11 does not show the strong forward and backward peaks which would be expected from this channel, which decays into an $L = 4$ state. A t-channel process involving A2 exchange is possible, but this is not expected to be the dominant process just above threshold.

C. η' Production in the 3- and 4-prong Events

Those η' events in which the η decays neutrally are found in the 3- and 4-prong events; from equation (14), 34% of the η' events are in the final state $pp\pi^+\pi^-(\eta,\ \eta \to \text{neutrals})$.

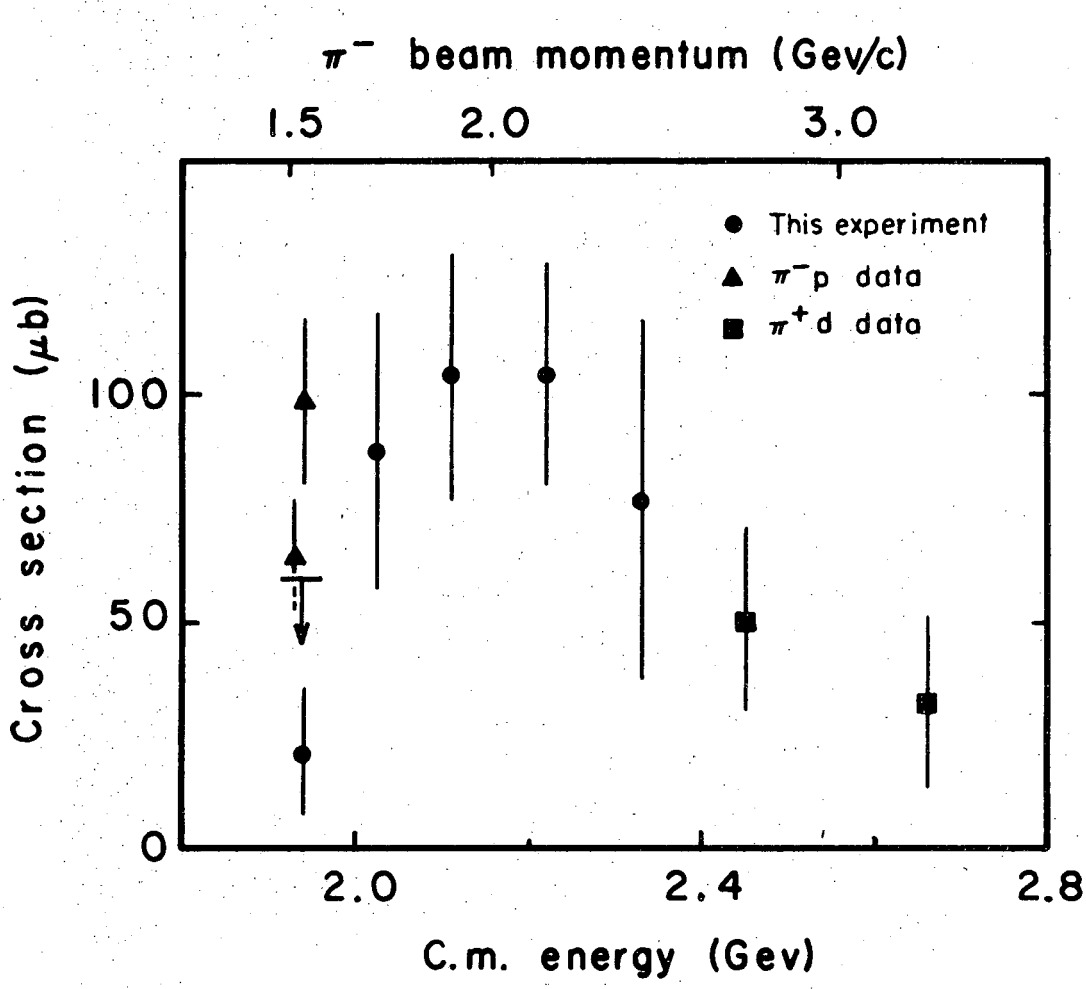

Figure 10. Cross section for $\pi^+ n \rightarrow p\eta'$; the charge-symmetric data and $\pi^+ d$ data are also shown.[28]

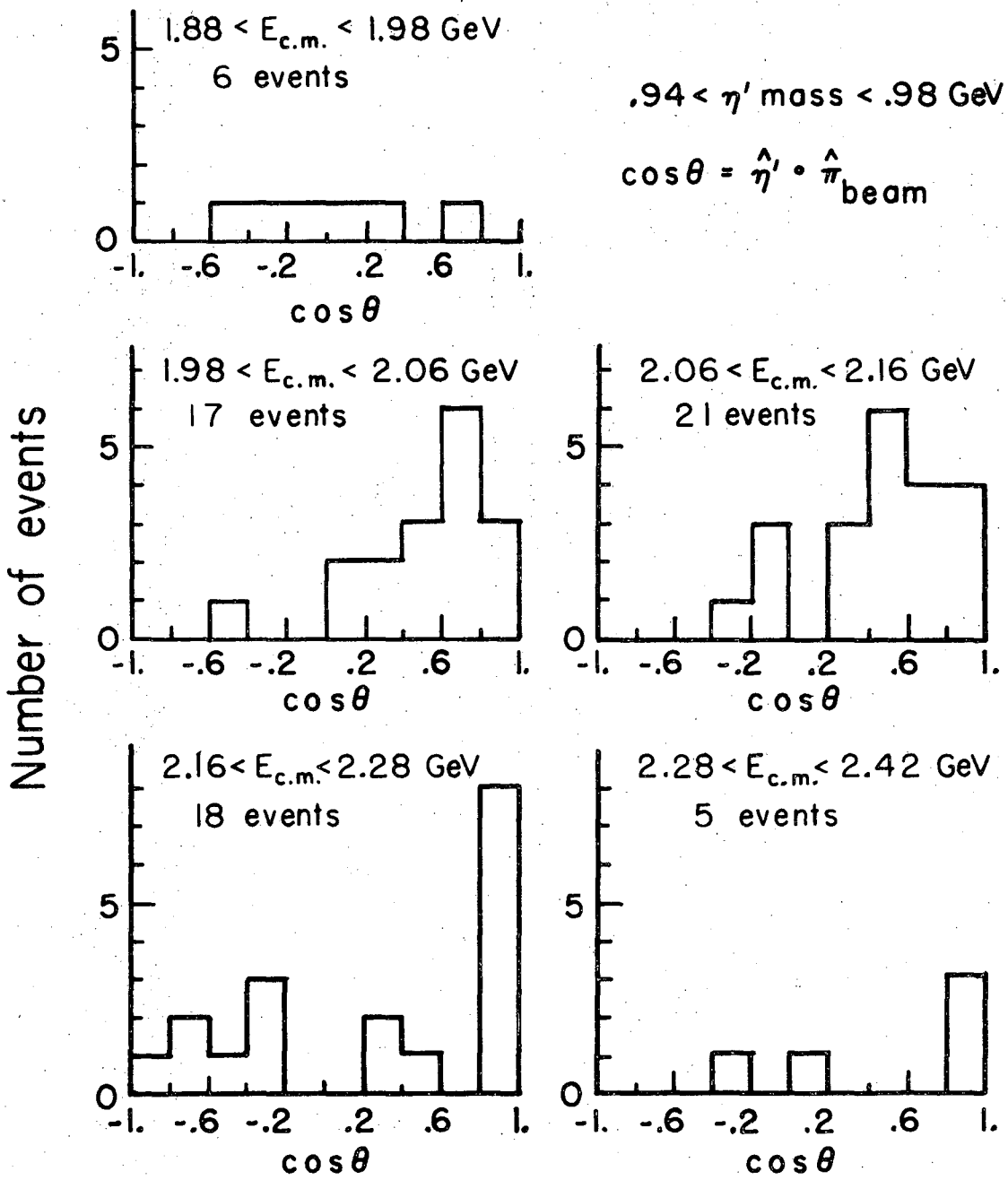

Figure 11. η' production cosine in c.m. frame, for the 5- and 6-prong events.

Most of the 3- and 4-prong events have been analyzed elsewhere.[1,29] The events of interest are those with a missing mass = η mass (within errors), and which have no satisfactory fits to other hypotheses. We have examined this sample of events for evidence of η' production. The same cuts were made on the fiducial volume as for the 5- and 6-prong events. The 3- and 4-prong events were measured on the Spiral Reader, and the pulse height information was used to separate the track-mass hypotheses. The kinematic and ionization confidence levels for the accepted hypothesis are required to be greater than 1%. For this study, we also require that the spectator proton momentum be less than 0.25 GeV/c.

The missing mass of 3-prong events with a missing mass between 0.45 and 0.64 GeV/c^2 is shown in Figure 12; the missing mass of the 4-prong events with a missing mass between 0.5 and 0.6 GeV/c^2 is shown in Figure 13. There is no evidence for neutral η mesons in Figure 12; however we estimate that there are 70 to 100 events in the peak at the mass of the η meson in Figure 13.

The events shown in Figures 12 and 13 have been fit to the one-constraint hypothesis $\pi^+ d \rightarrow pp\pi^+\pi^-\eta$, $\eta \rightarrow$ neutrals. The scatterplot of missing mass versus the $(\pi^+\pi^-\eta)$ mass is shown in Figure 14 for the 3-prongs, and in Figure 15 for the 4-prongs. There is a good η' signal in both these plots; the plots also show that the background can be reduced if we make a more restrictive cut on the acceptable missing η hypothesis. For the rest of the analysis

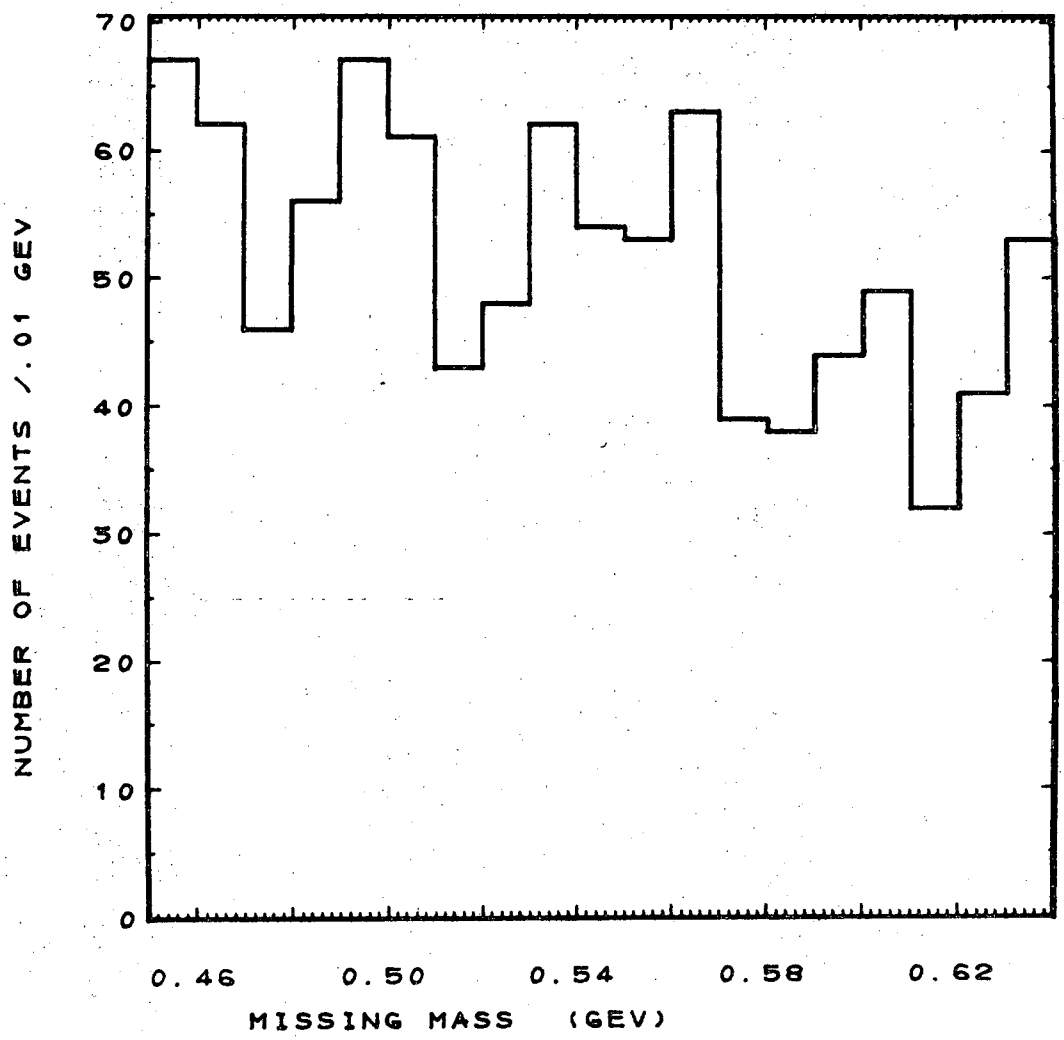

Figure 12. Missing mass for selected 3-prong events (978 events).

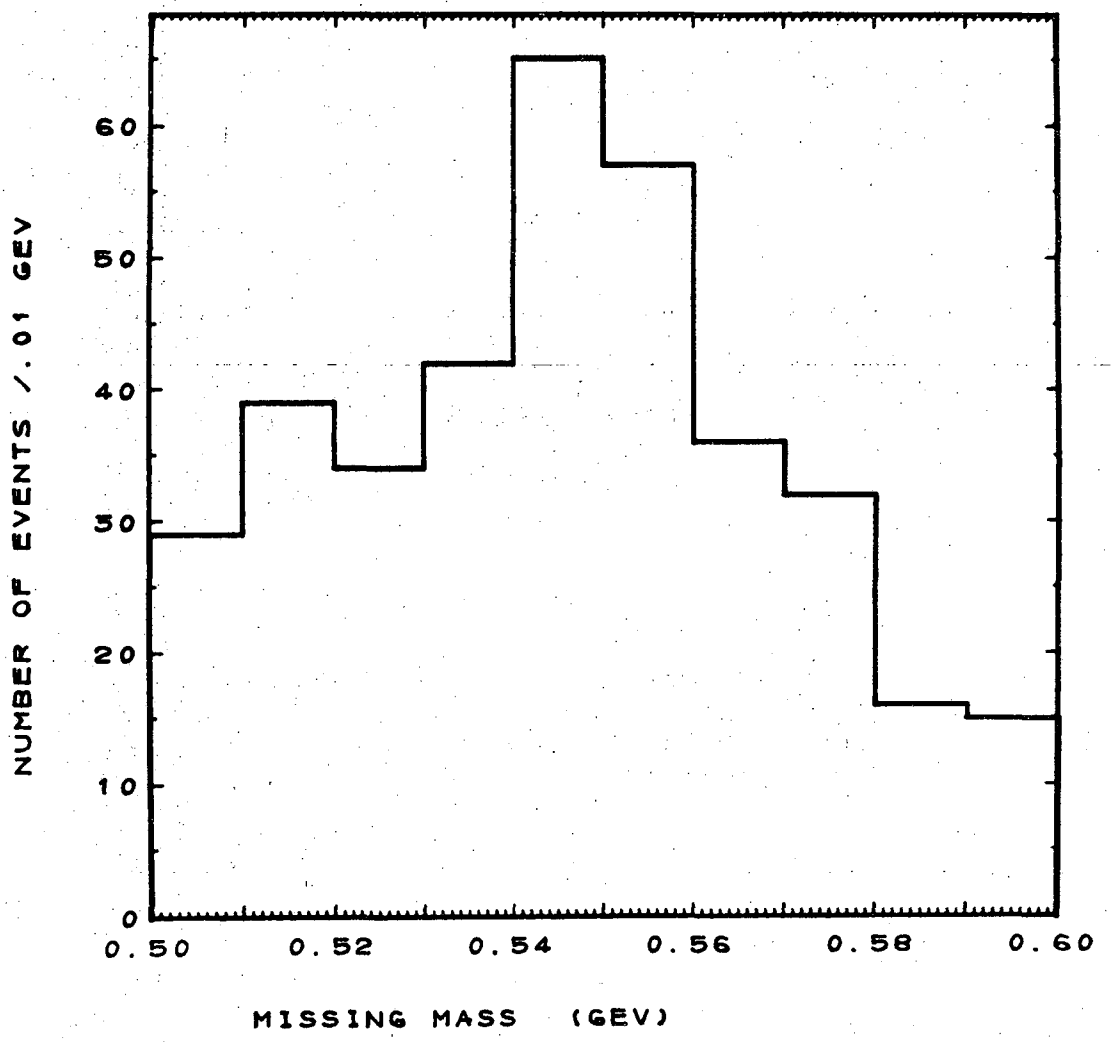

Figure 13. Missing mass for selected 4-prong events (365 events).

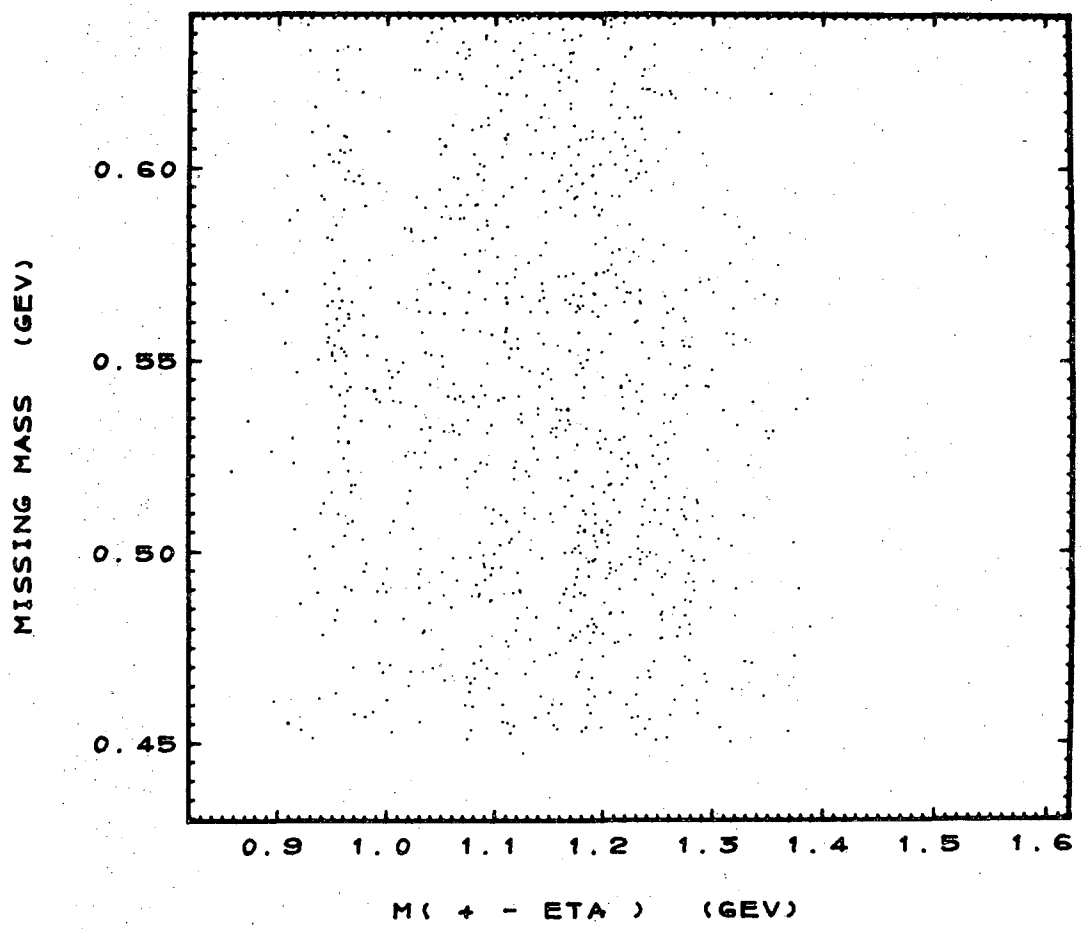

Figure 14. Missing mass vs. $M(\pi^+\pi^-\eta)$ for selected 3-prong events (888 events).

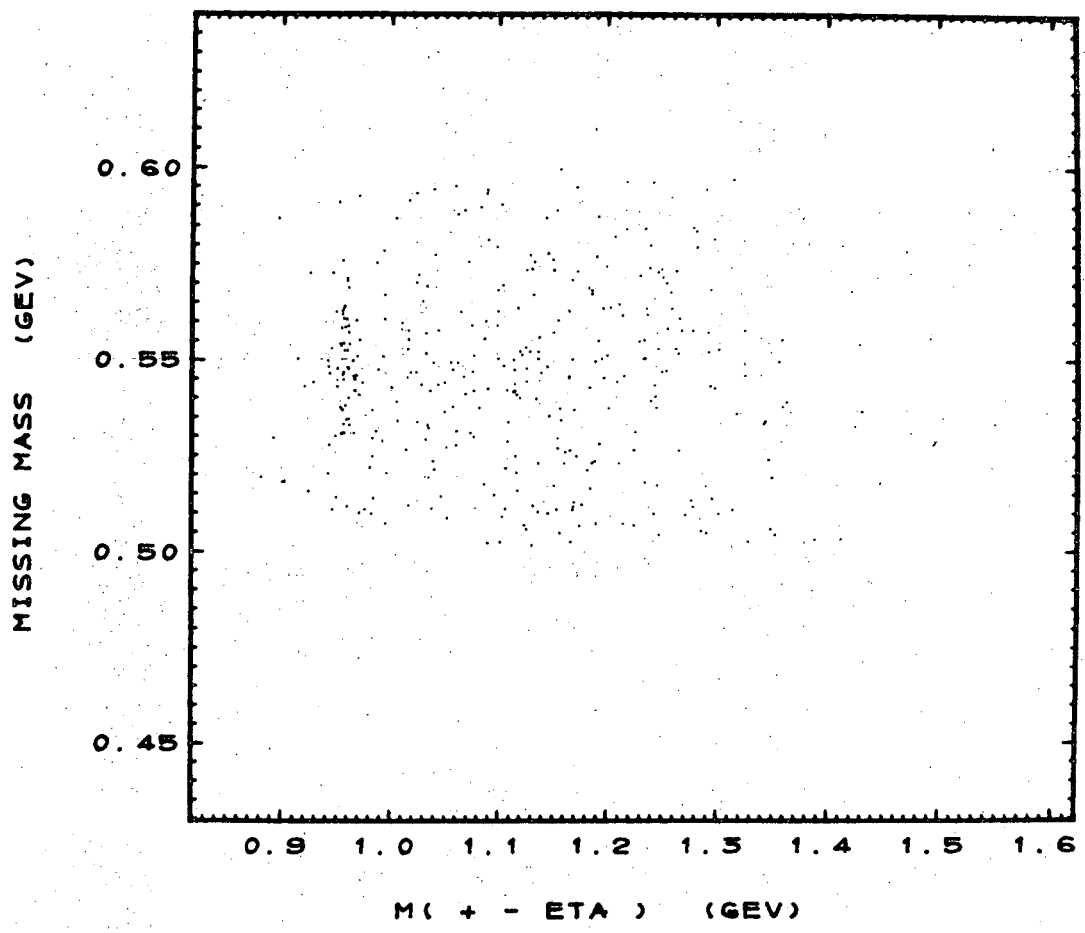

Figure 15. Missing mass vs. $M(\pi^+\pi^-\eta)$ for selected 4-prong events (359 events).

we require that the missing mass lie between 0.50 and 0.64 GeV/c^2 in the 3-prongs, and between 0.52 and 0.58 GeV/c^2 in the 4-prongs.

The scatterplot of c.m. energy versus the $(\pi^+\pi^-\eta)$ mass is shown in Figures 16 and 17 for the 3- and 4-prong events, respectively. The $(\pi^+\pi^-\eta)$ mass projections are also shown in Figures 16 and 17. The η' peak is sharp and clear here, even for the 3-prong events. The background under the η' peak is about 20% for both topologies. The amount of η' production was determined as a function of c.m. energy; the number of η' events is tabulated in Table 13.

The number of η' events observed in the same c.m. energy interval in the 5- and 6-prong events is also tabulated in Table 13, as well as the ratio of η' events seen in the 3- and 4-prongs to those seen in the 5- and 6-prongs. If the detection efficiency were the same for both samples, we expect a ratio of 2.5. The overall observed ratio is 3.2 ± 0.7.

The cross section for η' production has been estimated for the 4-prong events: by interpolating the pathlength distribution given in ref. 1, pp. 76 and 77 we find the pathlength values given in Table 14. These pathlengths are for 4-prong events with the same quality cuts which we have applied, but with a spectator momentum cut at 300 MeV/c. From the figures in ref. 1, we estimate that these pathlength values are approximately 10% too high. The cross sections calculated using these pathlengths are also given in Table 14; these values agree with those given in Table 12, except at 2.03 GeV.

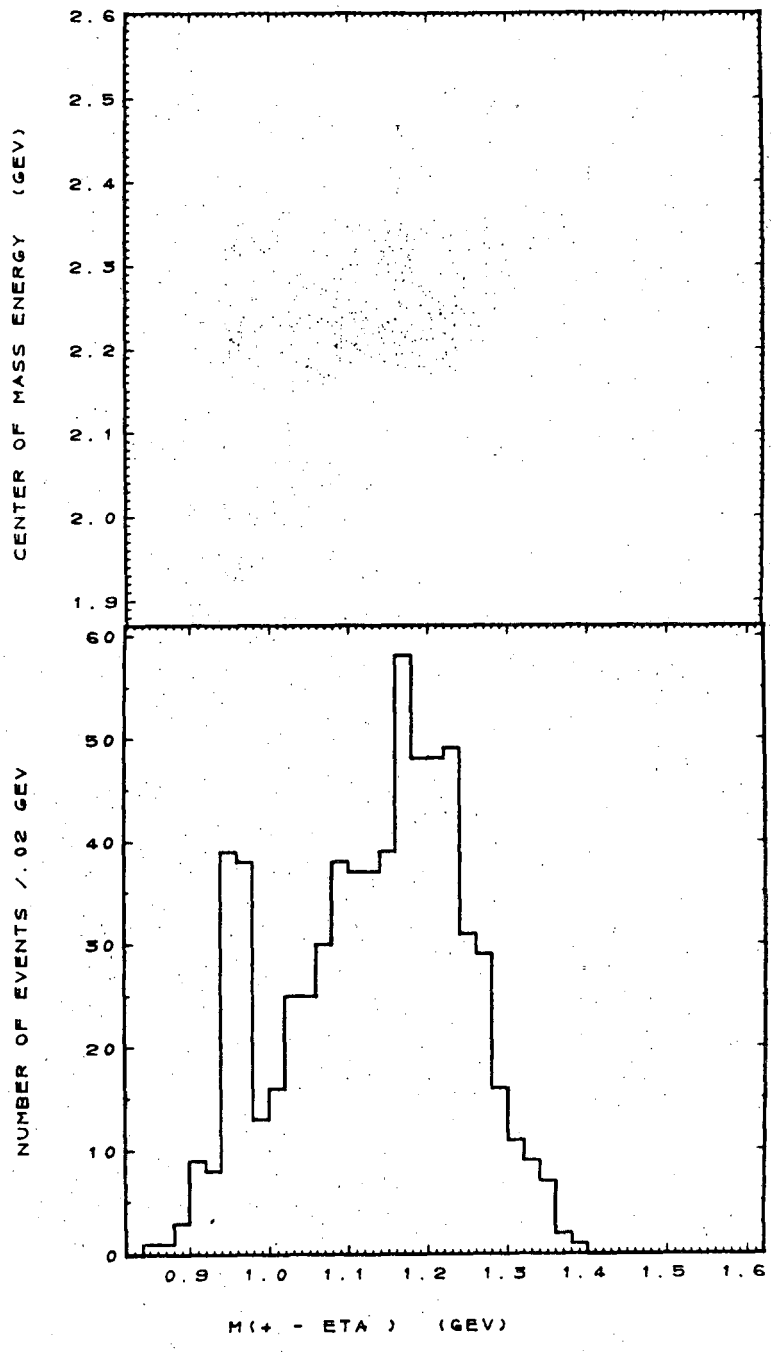

Figure 16. C.m. energy vs. $M(\pi^+\pi^-\eta)$ for selected 3-prong events, with missing mass cut (668 events).

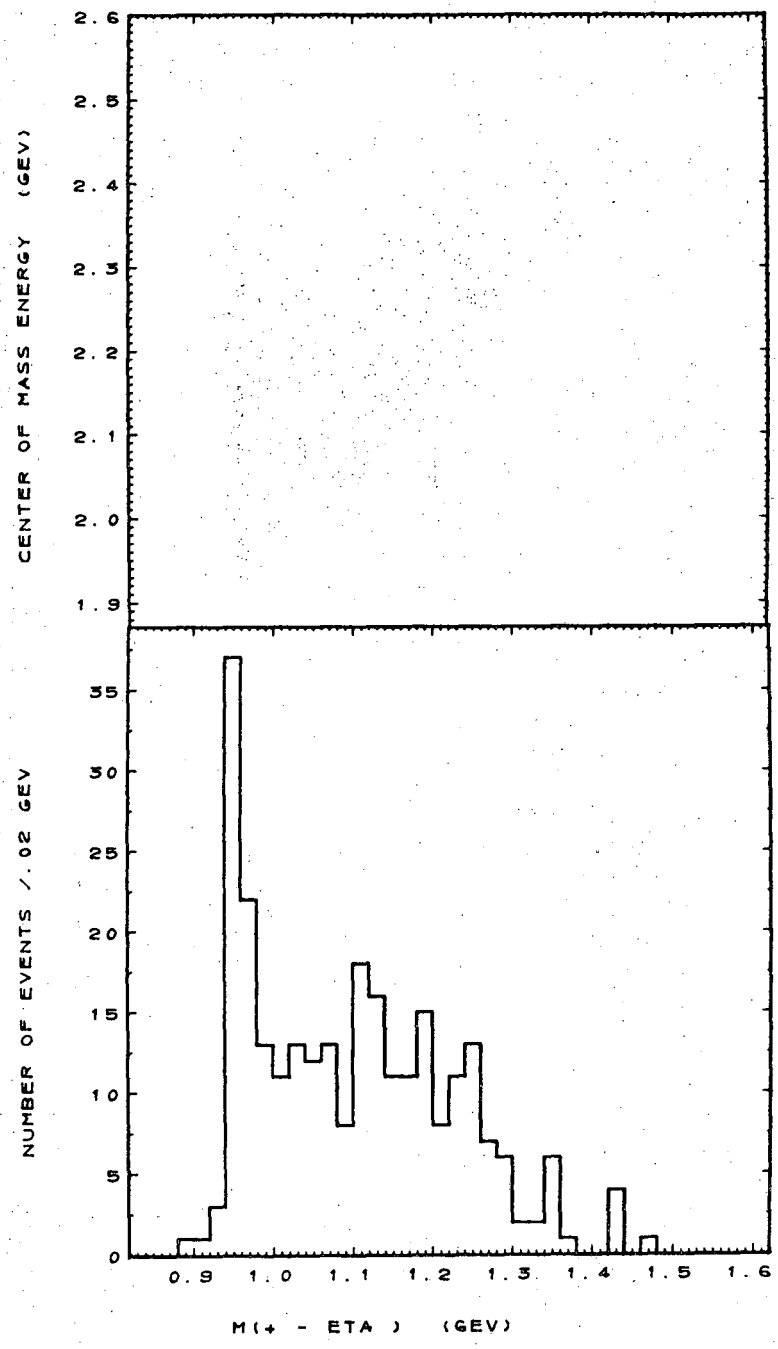

Figure 17. C.m. energy vs. $M(\pi^+\pi^-\eta)$ for selected 4-prong events, with missing mass cut (266 events).

Table 14. Estimated η' cross section, from the 4-prong events.

$E_{c.m.}$ (GeV)	1.94	2.03	2.11	2.22	2.33
Pathlength (evt/μb)	0.307	0.368	0.407	0.337	0.172
$\sigma_{observed}$ (μb)	16 ± 8	5 ± 4	59 ± 17	26 ± 10	17 ± 11
σ_{total} (μb)	48 ± 23	16 ± 12	173 ± 50	79 ± 31	51 ± 31

Table 15. Forward-backward ratios for the $\pi^+\pi^-\eta$ system.

$E_{c.m.}$ (GeV)	1.94	2.03	2.11	2 22	2.33
5-, 6-prong η'	1 ± 1	16 ± 16	4 ± 2	2 ± 1	4 ± 4
5-, 6-prong background	(0/2)	2 ± 1	2 ± 1	2 ± 1	1 ± 1
3-, 4-prong η'	2 ± 1	3 ± 2	7 ± 5	4 ± 1	16 ± 16
3-, 4-prong background	0.9 ± 0.3	0.8±0.3	1.4±0.4	2.7±0.4	1.8±0.5

Nothing is gained by attempting to fold the two sets of values together, due to the systematic uncertainties.

The η' production angular distribution was studied by making a cut on the $(\pi^+\pi^-\eta)$ mass between 0.94 and 0.98 GeV/c^2. The production angular distributions for the 3- and 4-prong events are consistent with each other. The production angular distributions for the 3- and 4-prong events in the η' mass region are shown in Figure 18.

No background subtractions have been made on these angular distributions. There is qualitative agreement between the background angular distribution and that of the η' events. In order to make a quantitative comparison of the η' angular distribution with that of the background, we calculate the ratio of the number of events going forward ($\cos > 0$) to those going backward ($\cos < 0$). This ratio is caluclated for each $E_{c.m.}$ bin; the background events used are those not in the η', with $(\pi^+\pi^-\eta)$ mass less than 1.1 GeV/c^2. These ratios are shown in Table 15. There is no significant difference between the background and the signal. The same procedure has been carried out with the 5- and 6-prong events, with the same result. These ratios are also given in Table 15.

The data for all of the η' events is summarized in Figures 19 and 20. Figure 19 shows the $(\pi^+\pi^-\eta)$ mass plot. Only 5- and 6-prong events which have at least one $(\pi^+\pi^-\pi^0)$ mass in the η region (0.53 $M(\pi^+\pi^-\pi^0)$ 0.59 GeV/c^2) are used. Figure 20 shows the angular distributions for all of the η' events.

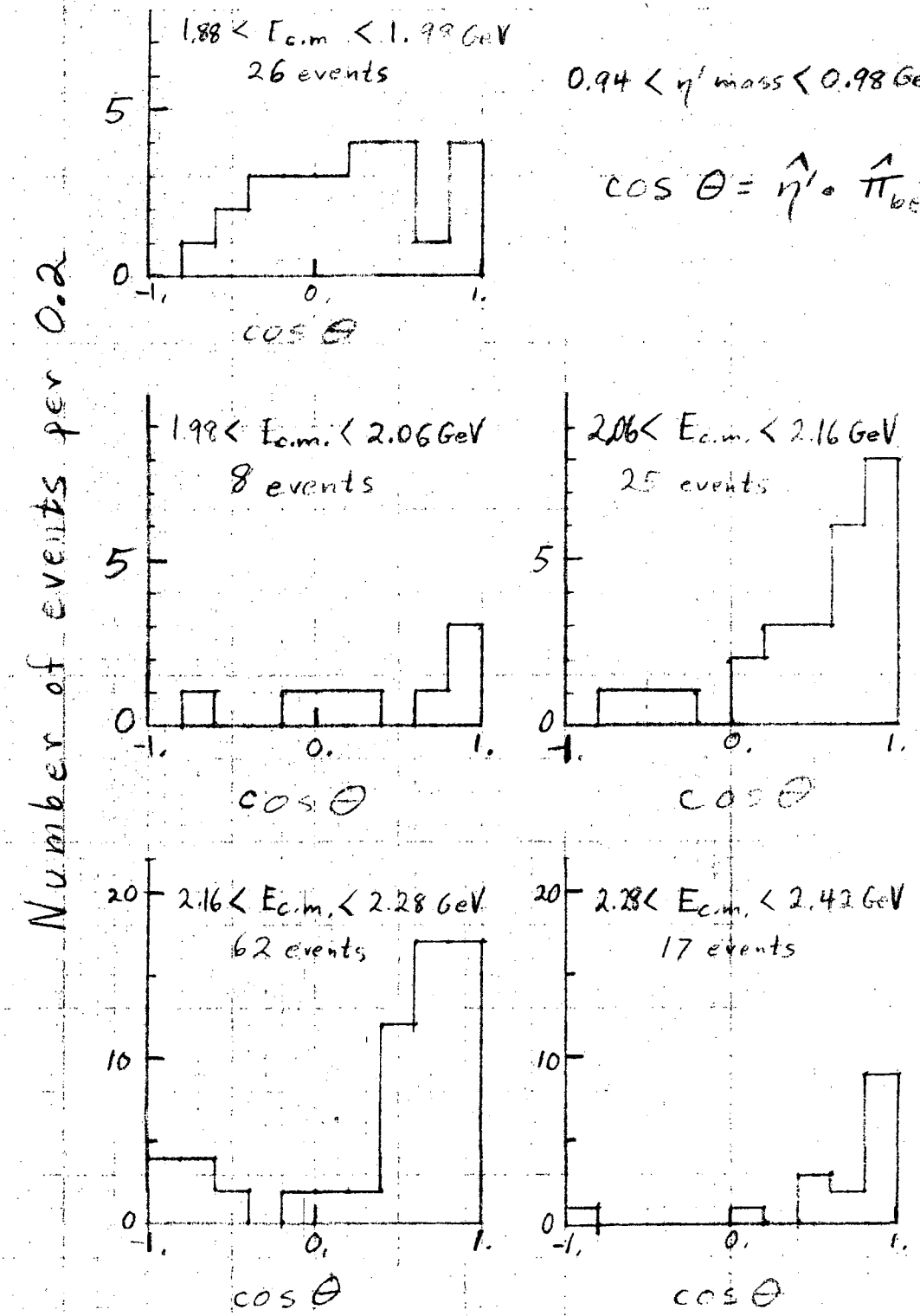

Figure 18. η' production cosine in c.m. frame for 3- and 4-prong events.

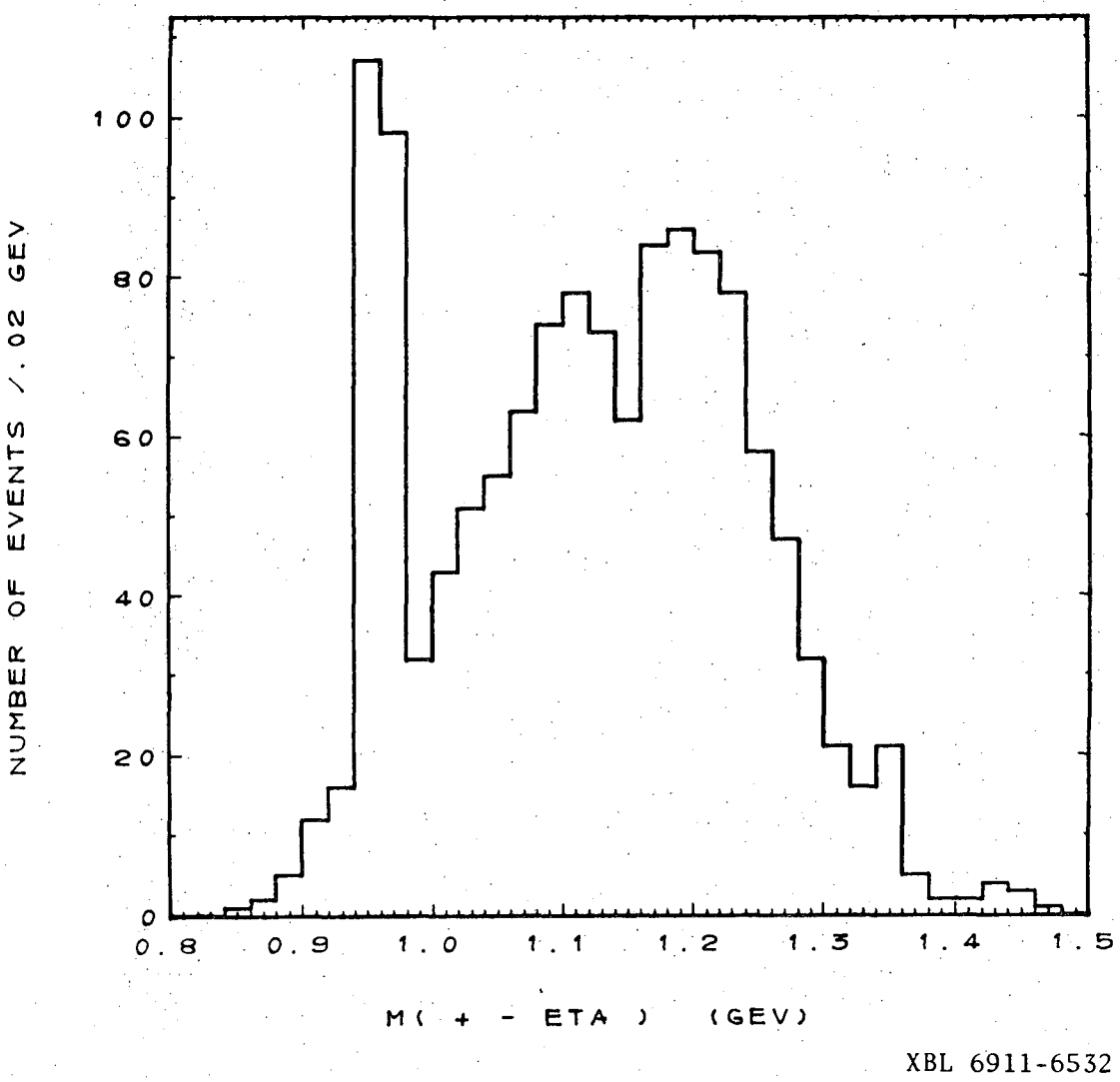

Figure 19. $M(\pi^+\pi^-\eta)$ for 3-, 4-, 5-, and 6-prong events (1315 events).

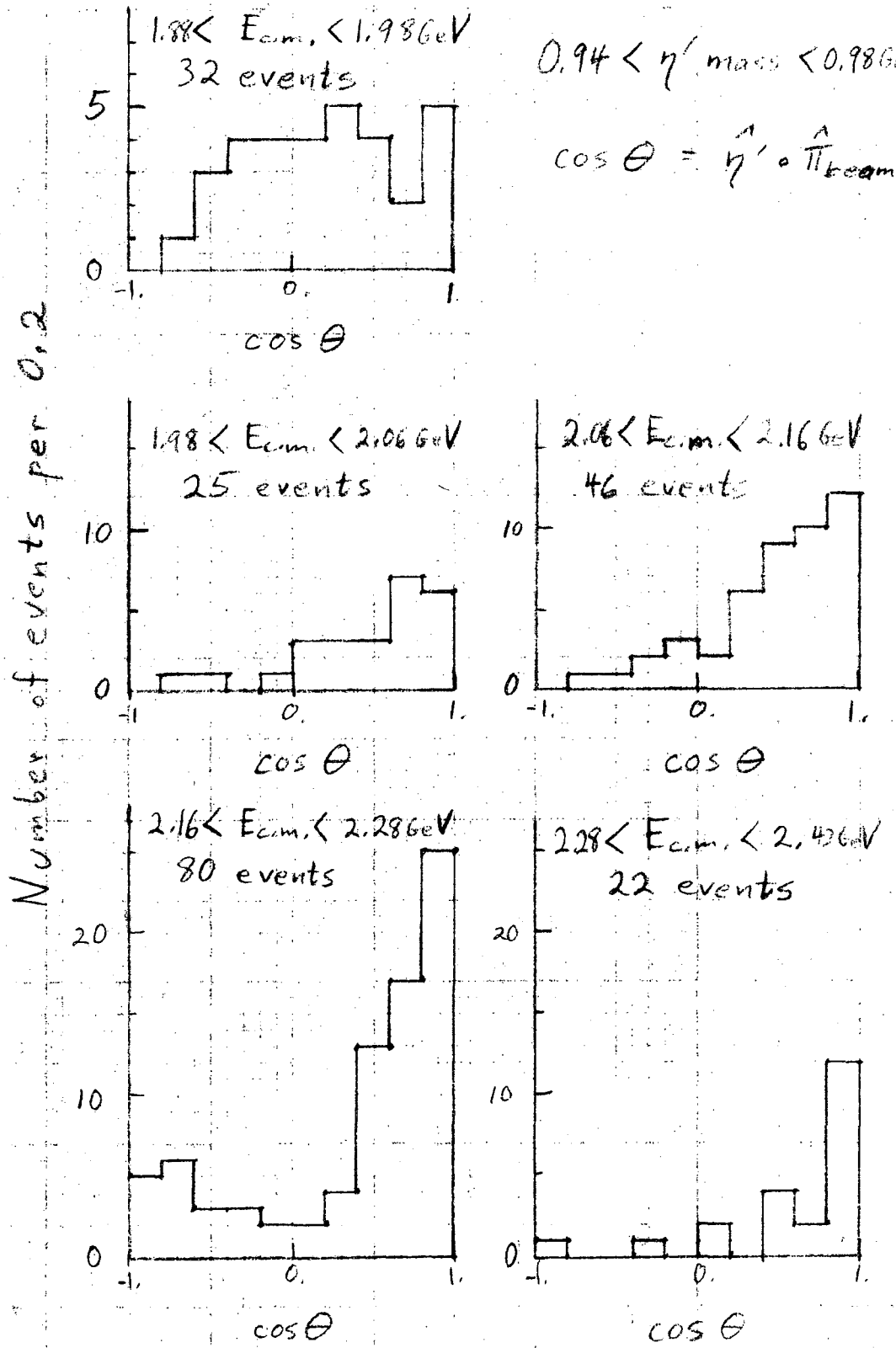

Figure 20. η' production cosine in c.m. frame, for 3-, 4-, 5- and 6-prong events.

VI. SUMMARY OF RESULTS

The cross section for η' production in the reaction $\pi^+ n \rightarrow p\eta'$ has been determined, from threshold to 2.4 GeV/c. These cross sections, and the charge-symmetric cross sections from other experiments, are shown in Figure 10. The production angular distribution (Figure 11) shows that the s-channel resonance process $\pi^+ n \rightarrow N^*_{1/2}(2190) \rightarrow p\eta'$ is not dominant; a t-channel process involving A2 exchange is possible, but there is not enough data to warrant an attempt to model A2 exchange.

ACKNOWLEDGEMENTS

This work would not have been possible without the cooperation of many people, and the understanding support of my wife. Special thanks are due to the crews of the Bevatron and the 72-in. bubble chamber. The scanning and measuring were accomplished under the supervision of Wally Hendricks.

It is a pleasure to acknowledge many useful discussions with Don Davies and Paul Hoch, and the advice and encouragement of Profs. Donald Miller and Janos Kirz.

Finally, I acknowledge the support and example of Professor Luis Alvarez, without which this work would not have been possible.

This work was done under the auspices of the U. S. Atomic Energy Commission.

APPENDIX A. DISTRIBUTING THE PATHLENGTH IN C.M. ENERGY

We know our pathlengths at each of our several beam momenta; we would like to know how much pathlength we have as a function of the c.m. energy of the πN system. We use the spectator model to give us an explicit way of calculating the distribution of the pathlength in c.m. energy.

We approximate the deuteron wave function by the Hulthen wave function.[11] The Hulthen wave function H(p) can be written as

$$H(p) = \frac{1}{p^2 + \alpha^2} - \frac{1}{p^2 + \beta^2} . \qquad (A1)$$

The value of α is determined by the deuteron binding energy to be $\alpha = 0.0457$ GeV/c. The value of α we use is calculated from the new value for the deuteron binding energy.[14] The parameter β determines how quickly the second term cancels the first, and thus can account for more or less high momentum spectators. In the literature β has been taken to be 7α[15] and 5.18α[16]. The value $\beta = 0.236$ GeV/c used here is the value from ref. 16. None of our results are senstive to the value of β.

The c.m. energy of the πN system is given by

$$E_{c.m.} = \sqrt{(P_b + P_t)^2} , \qquad (A2)$$

where P_b is the four-vector of the beam particle, and P_t is the four-vector of the target, given experimentally by

$P_{deuteron} - P_{spectator}$. The invariant flux factor[12] is

$$Flux(p_b, p_t, x) = \sqrt{(P_b \cdot P_t)^2 - m_b^2 m_t^2} \; / m_b m_t \qquad (A3)$$

where p_b, p_t are the magnitudes of the beam and target momenta, and $x = \vec{p}_b \cdot \vec{p}_t / p_b p_t$.

Thus the probability density for incident beam particles with momentum p_b to approach the target with $E_{c.m.} = E$ is

$$P(E, p_b) = Const. \int |H(p)|^2 Flux(p_b, p_t, x) p_t^2 dp_t d\Omega_t \, \delta(E_{c.m.} - E) \; . \qquad (A4)$$

The incident flux is spread out in c.m. energy by the Fermi motion of the target, as is evident in equation (A4), and also by the momentum lost in traversing the chamber, and by the spread in the beam momentum. We have assigned widths to our beam momenta of ±1%; the momentum loss through the chamber is 40 MeV/c (the tracks are minimum ionizing). To take these effects into account, we define the function $f(p_b, p_i)$ to be the convolution of a Gaussian resolution function (width 1% of the beam momentum p_i) with a flat distribution in momentum due to energy loss in the chamber. Given the central value of the beam momentum distribution, p_i, $f(p_b, p_i)$ is the fraction of beam particles passing a nucleon target with momentum p_b.

Noting that

$$\int dp_b f(p_b, p_i) \int P(E, p_b) dE = 1 \; , \qquad (A5)$$

as these are normalized probability densities, we can write

$$\begin{aligned} PL &= \sum PL_i \\ &= \sum \int dp_b f(p_b, p_i) \int dE\ P(E, p_b) PL_i \\ &= \int dE \int dp_b \sum f(p_b, p_i)\ P(E, p_b) PL_i \end{aligned} \tag{A6}$$

where PL stands for pathlength, and the summation is over all of the beam momentum settings. Thus we can define

$$\frac{\partial PL(E)}{\partial E} = \int dp_b \sum PL_i f(p_b, p_i) P(E, p_b) \tag{A7}$$

to be the differential pathlength at energy E.

The pathlength in a given bin of c.m. energy is given by

$$PL = \int_{E_{low}}^{E_{high}} dE\ \frac{\partial PL}{\partial E}(E)\ . \tag{A8}$$

The c.m. energy bins which we have used, and the resulting pathlengths, are given in Table A.1.

Table A.1. Center of mass energy bins and pathlengths.

Lower Limit (GeV)	Central Value (GeV)	Pathlength (events/μb)
	(underflow)	0.04
1.68	1.73	0.42 ± 0.03
1.78	1.84	0.58 ± 0.04
1.88	1.94	2.62 ± 0.15
1.98	2.02	3.03 ± 0.17
2.06	2.11	3.09 ± 0.16
2.16	2.22	2.90 ± 0.13
2.28	2.33	1.02 ± 0.08
2.42	(overflow)	0.04

FOOTNOTES AND REFERENCES

1. Jerome S. Danburg, UCRL-19275 (Ph. D. thesis), 1969.
2. Donald W. Davies, UCRL-19263 (Ph. D. thesis), 1969.
3. See ref. 1, appendix A.
4. R. K. Rader, "Pathlength Determination in π66B", Lawrence Radiation Laboratory Physics Group A Physics Note No. 699 (unpublished).
5. Kirz, Hendricks et. al., "Scan Instructions for Multiprong Events: Experiment 25", Lawrence Radiation Laboratory Physics Group A Physics Note No. 597 (unpublished).
6. For a comparison of the performance of these measuring machines, see R. Rader, "Comparison of Franckenstein and Spiral Reader Measurements", Lawrence Radiation Laboratory Physics Group A Physics Note No. 677 (unpublished).
7. F. T. Solmitz, A. D. Johnson, and T. B. Day, "Three View Geometry Program", Lawrence Radiation Laboratory Physics Group A Programming Note P-117 (unpublished).
8. O. I. Dahl, T. B. Day, F. T. Solmitz and N. L. Gould, "SQUAW--Kinematic Fitting Program", Lawrence Radiation Laboratory Physics Group A Programming Note P-126 (unpublished).
9. Paul Hoch, "Range-Momentum Scale Factor and Index of Refraction for d_2 in the 72-in. B. C.", Lawrence Radiation Laboratory Physics Group A Physics Note No. 616 (unpublished).

10. See ref. 1, p. 132.

11. Lamek Hulthén and Masao Sugawara, in Handbuch der Physik (Springer-Verlag, Berlin, 1957), Vol. 39, Chap. 1--esp. Sections 13 and 53.

12. R. G. Newton, Scattering Theory of Waves and Particles (McGraw-Hill, 1966), Chap. 8, Sec. 2.

13. The cross sections for $\pi^- p \rightarrow n\pi^+\pi^+\pi^-\pi^-$ shown in figure 5 are given below, together with their sources.

a) $\sigma = 0.12 \pm 0.02$ mb at 1.59 GeV/c, from Saclay-Orsay-Bari-Bologna Collaboration, Nuovo Cimento 29, 515 (1963).

b) $\sigma = 0.34 \pm 0.11$ mb at 1.89 GeV/c, from R. Christian, A. R. Erwin, H. R. Fechter, F. E. Schwamb, S. H. Vegors, and W. D. Walker, Phys. Rev. 143, 1105 (1966).

c) $\sigma = 0.35 \pm 0.04$ mb at 2.03 GeV/c, from D. D. Carmony, F. Grard, R. T. Van de Walle, and Nguyen-huu Xuong, International Conference on High Energy Physics at CERN (1962), p. 44.

d) $\sigma = 0.37 \pm 0.02$ mb at 2.10 GeV/c, from P. H. Satterblom, W. D. Walker, and A. R. Erwin, Phys. Rev. 134, B207 (1964).

e) $\sigma = 0.67 \pm 0.02$ mb at 2.70 GeV/c, from P. R. Klein, R. J. Sahni, A. Z. Kovacs, and G. W. Tautfest, Phys. Rev. 150, 1123 (1966).

f) $\sigma = 0.66 \pm 0.03$ mb at 2.75 GeV/c, from J. Alitti, J. P. Baton, A. Berthelot, B. Deler, W. J. Fickinger, N. Neveu-Rene, V. Alles-Borelli, R. Gessaroli, A. Romano, and P. Waloschek, Nuovo Cimento 35, 1 (1965).

g) $\sigma = 1.0 \pm 0.1$ mb at 3.7 GeV/c, from W. D. C. Moebs, III, Ph. D. thesis, University of Michigan, 1965 (unpublished). (The value used was taken from a graph in Suh Urk Chung, Orin I. Dahl, Janos Kirz, and Donald H. Miller, Phys. Rev. 165, 1491 (1968).)

14. H. W. Taylor, N. Neff, J. D. King, Physics Letters 24 B, 659 (1967).

15. R. L. Gluckstern and H. A. Bethe, Phys. Rev. 81, 761 (1951).

16. M. Moravcsik, Nucl. Phys. 7, 113 (1958).

17. George R. Kalbfleisch, Luis W. Alvarez, Angela Barbaro-Galtieri, Orin I. Dahl, Philippe Eberhard, William E. Humphrey, James S. Lindsay, Deane W. Merrill, Joseph J. Murray, Alan Rittenberg, Ronald R. Ross, Janice B. Shafer, Frank T. Shively, Daniel M. Siegel, Gerald A. Smith, and Robert D. Tripp, Phys. Rev. Letters 12, 527 (1964).

18. M. Goldberg, M. Gundzik, J. Leitner, M. Primer, P. L. Connolly, E. L. Hart, K. W. Lai, G. W. London, N. P. Samios, and S. S. Yamamoto, Phys. Rev. Letters 13, 249 (1964).

19. Alan Rittenberg, UCRL-18863 (Ph. D. thesis), 1969.

20. Naomi Barash-Schmidt, Angela Barbaro-Galtieri, LeRoy R. Price, Arthur H. Rosenfeld, Paul Soding, Charles G. Wohl, Matts Roos, and Gianni Conforto, Rev. Mod. Phys. 41, 109 (1969).

21. G. H. Trilling, J. L. Brown, G. Goldhaber, S. Goldhaber, J. A. Kadyk, and J. Scanio, Physics Letters 19, 427 (1965).

22. J. P. Dufey, B. Gobbi, M. A. Pouchon, A. M. Cnops, G. Finocchiaro, J. C. Lassalle, P. Mittner, and A. Muller, Physics Letters 26B, 410 (1968).

23. E. Hyman, W. Lee, J. Peoples, J. Schiff, C. Schultz and S. Stein, Nevis report 155, Columbia University, N. Y. (1966).

24. H. O. Cohn, R. D. McCulloch, W. M. Bugg and G. T. Condo, Physics Letters, 347 (1966).

25. T. C. Bacon, W. J. Fickinger, D. G. Hill, H. W. K. Hopkins, D. K. Robinson and E. O. Salant, Phys. Rev. 157, 1263 (1967).

26. Maris A. Abolins, Orin I. Dahl, Jerome S. Danburg, Donald Davies, Paul Hoch, Janos Kirz, Donald H. Miller and Robert Rader, Heidelberg International Conference on Elementary Particles, 1967.

27. R. J. Miller, S. Lichtman and R. B. Willmann, Phys. Rev. 178, 2061 (1969).

28. The cross sections for $\pi^- p \rightarrow n\eta'$, and $\pi^+ d \rightarrow pp\eta'$ shown in Figure 10 are as follows:

a) $\sigma \leq 60$ μb, $\pi^- p$ at 1.5 GeV/c, from ref. 23.

b) $\sigma = 65 \pm 12$ μb, $\pi^- p$ at 1.50 GeV/c, and $\sigma = 98 \pm 18$ μb, $\pi^- p$ at 1.52 GeV/c, from ref. 22.

c) $\sigma = 50 \pm 20$ μb, $\pi^+ d$ at 2.7 GeV/c, from ref. 27.

d) $\sigma = 30\ ^{+18}_{-11}$ μb, $\pi^+ d$ at 3.29 GeV/c, from ref. 24.

29. Robert J. Manning, UCRL-19339 (Ph. D. thesis), 1969.

TECHNICAL INFORMATION DIVISION
LAWRENCE RADIATION LABORATORY
UNIVERSITY OF CALIFORNIA
BERKELEY, CALIFORNIA 94720